

Vibration analysis of a SWATH-type ship

by

Platon Michael Velonias

Submitted to the Departments of Ocean Engineering
and Mechanical Engineering
in partial fulfillment of the requirements for the degrees of

Ocean Engineer

and

Master of Science in Mechanical Engineering

at the

MASSACHUSETTS INSTITUTE OF TECHNOLOGY

June 1995

© Massachusetts Institute of Technology 1995. All rights reserved.

Author
Department of Ocean Engineering
May 12, 1995

Certified by
Alan J. Brown, Professor of Ocean Engineering
Thesis Reader, Department of Ocean Engineering

Certified by
Klaus-Jürgen Bathe, Professor of Mechanical Engineering
Thesis Supervisor, Department of Mechanical Engineering

Accepted by
Ain A. Sonin, Professor of Mechanical Engineering
Chair, Departmental Committee on Graduate Students

Accepted by
A. Douglas Carmichael, Professor of Power Engineering
Chair, Departmental Committee on Graduate Students

MASSACHUSETTS INSTITUTE
OF TECHNOLOGY

JUL 28 1995

LIBRARIES

Vibration analysis of a SWATH-type ship

by

Platon Michael Velonias

Submitted to the Departments of Ocean Engineering and Mechanical Engineering
on May 18, 1995, in partial fulfillment of the
requirements for the degrees of
Ocean Engineer
and
Master of Science in Mechanical Engineering

Abstract

The purpose of this thesis is the investigation of vibrations in SWATH-type ships. This new type of ship has been developed during the last decade and looks like a catamaran with its two hulls fully submerged.

The vibrational analysis was performed in three phases:

In the first phase (vibrations due to regular waves) potential flow theory was used to build a code which simulates the sea environment and calculates the pressure distribution on the hull due to waves. The ship structure was modelled using the ADINA finite element code. Stresses were evaluated for different wave frequencies and the ship's headings and speeds. It was found that fatigue loads were low for a ship with a 20 years life span.

In the second phase (vibrations due to irregular waves) the natural frequencies of the structure were evaluated using the finite element ADINA code. The natural frequencies were found to be low when compared with the sea-wave spectrum, thus irregular waves will not diminish the ship's life (as it is dictated by fatigue loads).

In the third phase, vibrations due to the propeller working in a non-uniform flow were investigated. The propeller's loads were calculated using the PLL (propeller's lifting line) code. The ship's vibrational response was evaluated by modelling the ship structure and the shaft mounting using the ADINA code. The vibrational amplitudes were found to be within the norms of the classification societies.

Thesis Supervisor: Klaus-Jürgen Bathe
Title: Professor of Mechanical Engineering



Institute Archives and Special Collections
Room 14N-118
The Libraries
Massachusetts Institute of Technology
Cambridge, Massachusetts 02139-4307

**This is the most complete text of the thesis
available. The following page(s) were not included
in the copy of the thesis deposited in the Institute
Archives by the author: 3**

Contents

1	Introduction.	11
1.1	Swath ships	11
1.2	Vibrations in ships.	14
1.3	About this thesis.	18
2	Hydrodynamic analysis	19
2.1	Body response in regular waves	19
2.2	Calculating the velocity potentials	20
2.3	Numerical method	22
2.4	Program structure	28
2.5	Results	29
3	Description of SWATH ship structure	31
3.1	Main configuration	31
3.2	Finite element investigation	40
3.3	Fatigue loads.	49
3.3.1	Fatigue fracture.	51
3.3.2	Accumulative fatigue load calculation	53
3.4	Natural frequencies	55
4	Propeller vibrations	58
4.1	Procedure of vibration's measurement	58
4.2	Structure configuration	58

4.3	Propeller forces	61
4.3.1	Results.	64
5	Conclusions	67
A	Plates and stiffeners catalog.	71
B	Data for calculation of propeller loads.	73
C	Fatigue load calculations.	76
D	Propeller data.	78

List of Tables

3.1	Impact of design on stress concentration.	40
3.2	Wave spectrum of North Atlantic.	54
4.1	Propeller description.	60
C.1	New wave spectrum.	76
C.2	Resultant stress in [$\frac{lb}{ftsec^2}$]for given frequency and wave height.	77
D.1	Propeller data.	79

List of Figures

1-1	Ship vibrations.	16
1-2	Excitation sources.	17
1-3	Propeller forces.	17
2-1	Heaving amplitudes for different headings-wave frequencies.	30
2-2	Heaving amplitudes for different headings-wave frequencies.	30
3-1	General views.	34
3-2	Mid-section and detail.	35
3-3	Locations of Longitudinal and Transverse cross sections for the design of ship structure.	36
3-4	Midsection at $L/2$	37
3-5	Midsection at $L/4$ and $3L/4$	38
3-6	Diagram of plates and stiffeners.	39
3-7	Midsection (notch design).	41
3-8	Midsection (Radius =4 ft).	42
3-9	Midsection (radius=9 ft).	43
3-10	Midsection (finer mesh).	44
3-11	Stress distribution on mid-section.	45
3-12	Stress σ_{xx} (transverse direction).	47
3-13	Stress σ_{xx} (transverse direction).	47
3-14	Stress σ_{yy} (vertical direction).	48
3-15	Stress σ_{yy} (vertical direction).	48

3-16	“S-N” curves for annealed medium carbon steel.	52
3-17	Natural frequencies, modes 7,8 and 9.	57
4-1	Shafting arrangement.	59
4-2	Axial wake velocities.	62
4-3	Radial wake velocities.	62
4-4	Tangential wake velocities.	63
4-5	Blade load for each rotation angle.	63
4-6	Total perpendicular force acting on propeller’s shaft.	64
4-7	Deformation of upper deck due to propeller vibrations.	65
4-8	ISO Amplitude Evaluation Guidelines.	66

Glossary

- L_{bp} : Length between perpendiculars. The “perpendiculars” are straight lines perpendicular to the designed load waterline of a ship through a fixed point as stated by classification rules. Specifically:
 - i) aft or after perpendicular (AP) : through a fixed point at the stern; generally the aft side of the stern post, or center line of the rudder stock in ships without a stern post.
 - ii) forward perpendicular (FP): through a fixed point at the bow; generally the intersection of the fore side of the stem with the load waterline. [1]
- appendages : The portions of a vessel extending beyond the main hull outline, including such items as rudder, shafting, struts, bossings, and bilge keels struts.[1]
- heave (-ing): The vertical oscillatory motion of a specified point in a vessel (when it operates in waves), usually the center of the gravity. [1]
- Rolling: The angular component of the oscillatory motion of a ship measured about a longitudinal axis.[1]
- Pitching: The angular component of the oscillatory motion of a ship measured about a transversal axis.[1]
- Heading or wave encounter: The angle between the longitudinal axis of the ship and the direction of the wave encounter. [1]
- Slamming: Heavy impact resulting from a vessel’s bottom forward making sudden contact with the sea surface after having risen in a wave. Similar action results from rapid immersion of the bow in vessels with large flare.
- Springing: A vibration of the complete vessel induced by wave forces in conjunction with the ship’s elastic properties. More pronounced in ships having a high length-to-depth ratio.[1]
- Whipping: The transient ship-hull vibration induced by impulsive excitation forces. For example, fore-bottom slamming, bow-flare slamming, and stern slamming.[1]

- Frictional resistance: The component of resistance associated with the expenditure of energy in viscous effects.[1]
- Wave resistance: The component of resistance associated with the expenditure of energy in wave making.
- Head seas,quartering seas,beam seas, following seas: The direction of propagation of the wave front form an angle of 180^0 (head seas), 45^0 or 135^0 (quartering seas), and 0^0 with the course of the ship.
- DWT :(Dead weight Ton) The weight of the cargo a ship can carry.
- mb : millibars (10^{-3} Bars). Pressure unit.
- Pontoons: In our case the two submarine-like lower hulls of a SWATH vessel.

Chapter 1

Introduction.

1.1 Swath ships

Displacement hull ships are severely affected by sea conditions ,which limit their speed and/or their area of operation. Over the past two decades a new hull form geometry has been developed which has better seakeeping characteristics than any previous ship design. It is popularly called a SWATH (small waterplane area twin hull) ship in the U.S. and Europe and a SSC (semi-submerged catamaran) in Japan.

DESCRIPTION : This ship design provides a platform relatively isolated from the effects of sea waves. Buoyancy is provided by two pontoons (twin hulls) which are totally submerged and well below the surface, thus minimizing wave-making resistance. The struts, which connect the lower hulls with the platform, minimize the impact of waves on the ship. The advantages of this new ship design are :

- Improved seakeeping in rough seas (less roll,heave, and pitch). This is its main advantage. ¹
- Reduced slamming in waves.
- Reduced deck wetness.

¹Actually a multipurpose SWATH ship would probably not perform any particular mission any better than monohulls. However, for certain missions , in particular those in which seakeeping quality is an overriding factor, an optimized SWATH design may be quite superior to an optimized monohull.

- Better crew effectiveness, safety, and operational availability in high sea states. Increased comfort of the passengers (due to the small vertical acceleration in low frequencies).
- Ability to maintain speed in high sea states.
- Excellent low speed manoeuvring (due to the wide separation of its lower hulls) and coursekeeping.
- Lower propeller cavitation and vibration as well as improved efficiency due to the more uniform wake.
- Compared to conventional (monohull) ships of the same displacement, SWATH ships were found to be 5-10% slower in calm seas, due to their higher frictional resistance. SWATH ships become faster from sea states 4 and higher, due to their lower wave resistance.
- Finally it should be added that seakeeping characteristics may be even further improved by adding stabilizers. The impact of stabilizers on the ship's motions is very large². As small changes on the angle of attack of the stabilizer's fins generate a large correction of the ship's motion, a very smooth ride is possible. The design of the control system is simple for the same reason - the fins' rotation occurs only in small angles - and thus can be accomplished by using classical lifting surface and linear optimal control theory.

This special design also presents certain disadvantages :

- Struts provide light damping and little added mass. To increase these, struts are designed to be placed at an angle (not vertical).
- Large bending moments occur causing high stresses at the joints between the struts and the platform. The primary hull loads occur in the transverse direction; therefore, a transverse framing system is the obvious choice.

²The effectiveness of the ship's motion control system (stabilizers) is measured by the ratio of the lift forces and moments of the control surfaces at a nominal angle of attack to the tons-per-inch immersion and moment to heel or pitch one degree.

- The design of a SWATH ship is more difficult than the design of a conventional mono-hull, since the hydrodynamic performance of a SWATH ship is sensitive to the detailed geometry of the hulls ³. The lack of established design procedures and the necessity of knowing the detail hull design from the early stages of the SWATH design (so as to minimize power requirements and estimate seakeeping performance characteristics) make it even more difficult.

³Reduction of over 30% of the drag by fairly subtle changes in the hull shape have been reported.[3]

1.2 Vibrations in ships.

The response of a ship excited by vibrational forces has long attracted the attention of shipbuilders. As the computers' memory and speed increased, and larger problems were able to be handled, a better understanding of the interaction between the ship and its environment was acquired.

The excitation forces due to which a ship vibrates may be grouped into two categories : periodic and random vibrations.

- **Periodic vibrations** : The sources of these excitations are the main engine, the main turbines and gearing, the engines and auxiliary apparatus, and the propeller. More specifically, as the propeller operates in a non-uniform wake and due to the passage of the blades close to the hull and its appendages, the propeller generates fluctuating hydrodynamic forces and moments. The frequency of these forces equals the blade frequency ⁴ and its higher harmonics. Propeller forces are generally categorized into two groups :

b. Hull pressure forces : the pressure forces excite the ship through the hull bottom surface adjacent to the propeller. The pressure forces are fully described by three components (see fig. 1.2). They are generated from the pressure variation caused by the passage of propeller blade tips close to the hull and its appendages. The hull pressure forces are expected to be affected by propeller-hull clearance , by blade loading, and by changes in the local pressure field around the blade. An increase of hull pressure forces of 20 to 40 times due to blade cavitation has been observed in certain cases.

a. Bearing forces : the bearing forces excite the ship through the propulsion shafting / bearing system, and are fully described by six components (see fig. 1.3). They originate from the non-uniformity of the wake in the plane of the propeller disc.

- **Random Vibrations** : Their origin is found at the wave impact on the ship. The impact may be short with high intensity (shocks, slamming), or smooth with larger

⁴The blade frequency equals : (propeller's R.P.M) x (number of blades).

duration (sea-swell). The hydrodynamic characteristics of the ship and its behaviour at rough seas (sea-keeping) play a major role in how large the resultant loads will be for a given sea-state. The loading conditions result in the local vibrations of the outside plating and its steel-work as well as of the bottom.

In the following figure the origin of the vibrations and the resultant response of the ship are shown [6].

VIBRATION

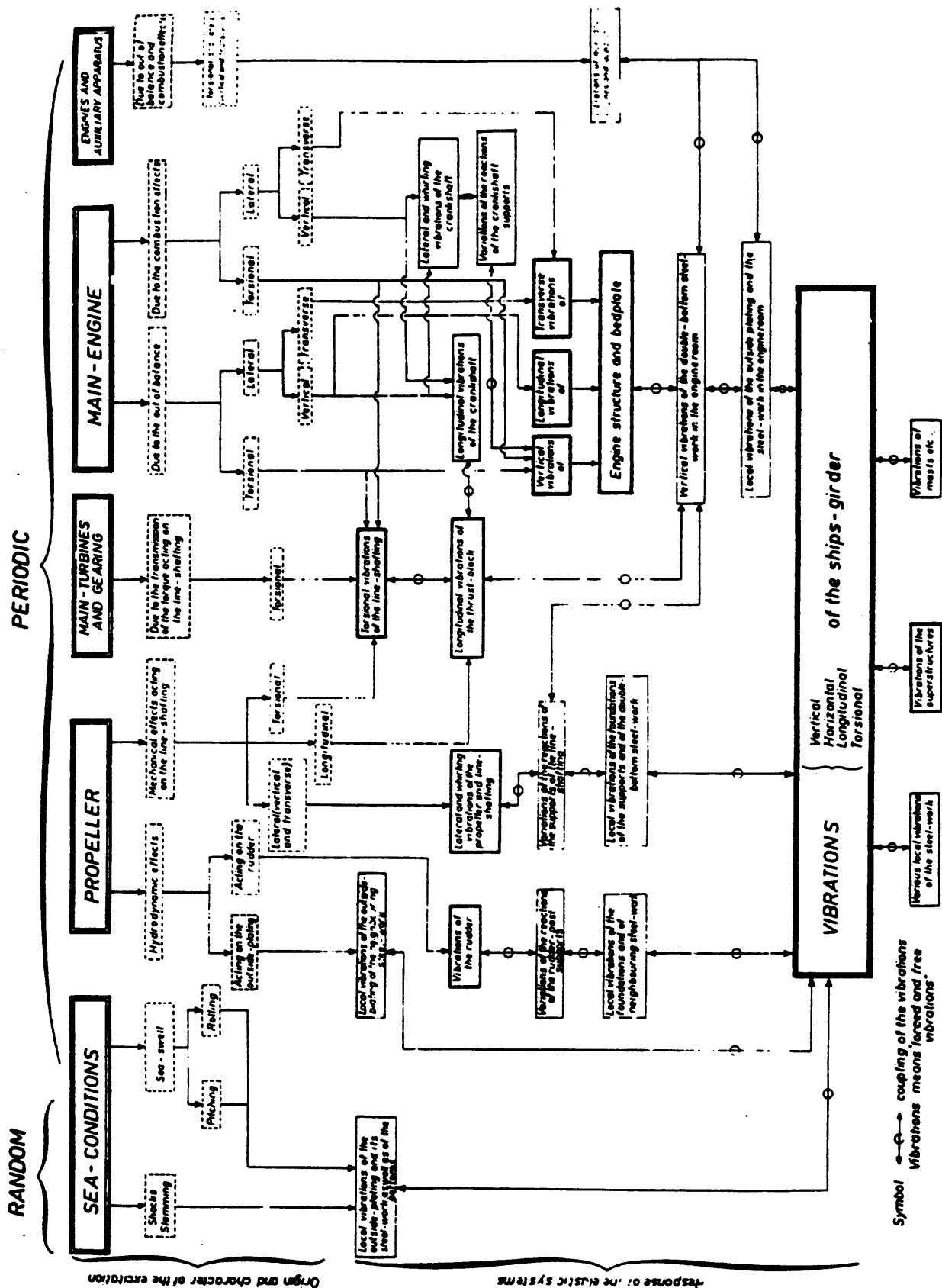


Figure 1-1: Ship vibrations.

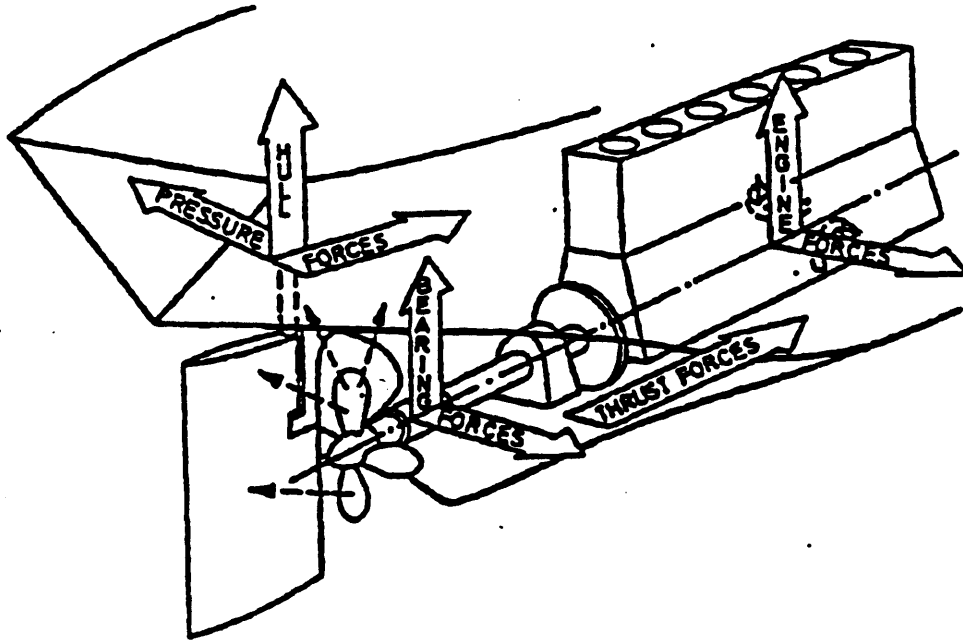


Figure 1-2: Excitation sources.

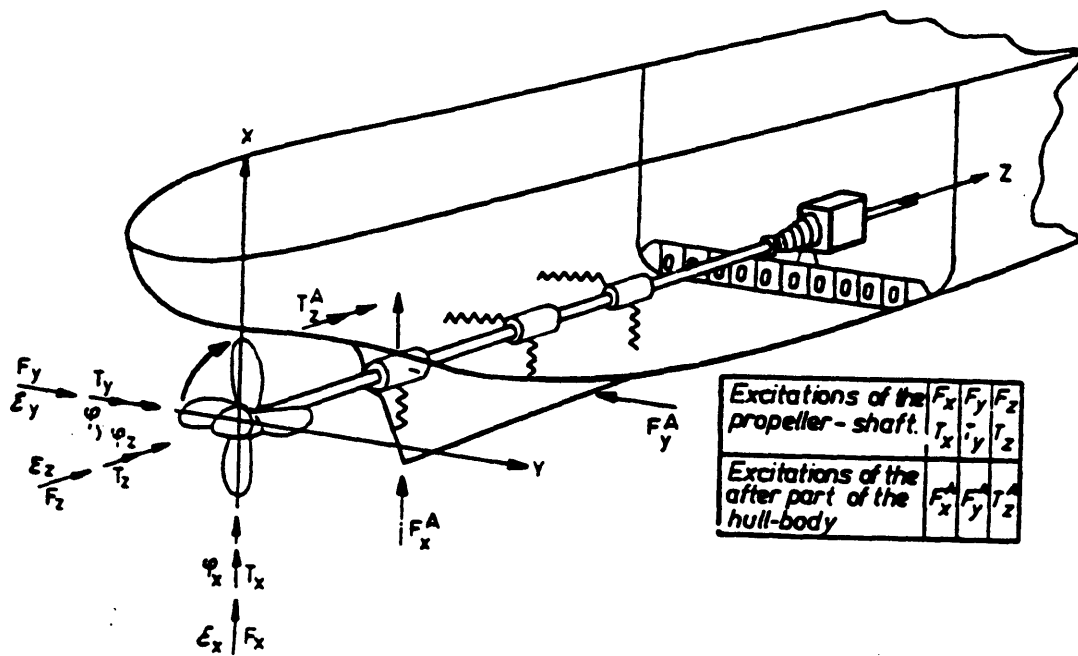


Figure 1-3: Propeller forces.

1.3 About this thesis.

The following chapters will examine the behavior of a SWATH ship in dynamic loading. More specifically the following aspects of the ship's excitation forces will be analyzed:

- **The wave-induced fatigue loads.** Chapter 2 will discuss the formulation of the problem of defining the pressure distribution around the ship's hull for different ship headings and speeds, and for different wave frequencies. Then, in chapter 3, after a brief description of the modelling of the structure of the ship, the wave-resultant stresses for each case will be calculated using the ADINA finite element code [5]. Finally, the accumulative fatigue load over the expected life of the vessel will be obtained.
- **The propeller-induced vibrations.** Although the magnitude of resultant stresses is not large enough to raise structural failure concerns, the produced noise level and velocity and acceleration amplitudes may well exceed the norms placed by the classifications societies.

In chapter 4, the forces resulting from the propeller functioning in a non-uniform wake will be calculated. Also, the modelling of the structure of the vessel will be described. Excitation loading of the finite element model [5] will be the blade frequency bearing forces input at the propeller.

As another approach the natural frequencies of the vessel [5] will be calculated and compared to the harmonics of the propeller-induced excitation (see section 3.4).

The next step will be the calculation of the response of the hull of the ship, i.e. amplitudes of velocity and acceleration at different points of the structure. The final step will be the comparison between the calculated vibration amplitude with the norms placed by the classification societies.

Chapter 2

Hydrodynamic analysis

2.1 Body response in regular waves

This section will describe the method used to define the pressure distribution around the two hulls.

As a first step in calculating the resultant stresses due to wave loading, the motion of the ship in regular waves was evaluated.

Assuming that superposition holds, two problems should be solved :

- **The radiation problem** : This problem consists of finding the potential ϕ_j ($j=1,2,\dots,6$) assuming a calm sea and a ship that oscillates in direction j with unit amplitude.
- **The diffraction problem** : This problem consists of finding the potential ϕ_A assuming that the ship is moving with constant forward speed U and that waves of frequency w_0 and unit amplitude propagate in direction θ relative to the ship's velocity.

We assumed plane progressive waves of small amplitudes, with sinusoidal time dependence, and wave amplitudes sufficiently small to justify linearization.

Therefore the corresponding velocities u_j of the translational and rotational motions (surge, heave, sway and roll, yaw, pitch) are expected to be sinusoidal in time with the same frequency.

$$\text{Thus : } u_j(t) = \text{Re}(i w \xi_j * e^{i w t})$$

For an incident wave with a small amplitude and a stable body, the resulting motions will be proportionally small. Thus, the velocity potential ϕ takes the form :

$$\phi(x, y, z, t) = Re[\sum_{j=1}^6 \xi_j \phi_j(x, y, z) + A \phi_a(x, y, z) * e^{i\omega t}] \quad (2.1)$$

Assuming that the velocity potential is a small first-order quantity, the distinction between the inertial coordinate system and one fixed in the body will be a source of second-order effects that can be neglected.

ϕ_j , $j = 1, 2, \dots, 6$ is the potential representing fluid motion resulting from forced body motion (oscillation with unit amplitude in direction j), in the absence of the incident waves. It can be calculated from the solution of the radiation problem.

The potential ϕ_a is due to the incident waves (ϕ_0) and their interaction with the body (ϕ_7). As the assumption of linear superposition holds, ϕ_a is independent of ship motion. It can be calculated from the solution of the diffraction problem.

2.2 Calculating the velocity potentials

This section will explore radiation and diffraction problems [3].

The radiation problem :

In 2D the problem to be solved is the following :

$$\nabla^2 \phi_j = 0 \quad (2.2)$$

with the following boundary conditions :

on the body surface :

$$\frac{\partial \phi_j}{\partial n} = i\omega n_j, \quad j = 2, 3 \text{ and} \quad (2.3)$$

$$\frac{\partial \phi_j}{\partial n} = i\omega (\vec{r} * \vec{n})_1, \quad j = 4 \quad (2.4)$$

radiation condition :

$$\phi_j \propto e^{\mp i k z}, z \rightarrow \pm \infty, j = 2, 3, 4 \quad (2.5)$$

on the free surface :

$$\left(\frac{\partial}{\partial t} - U \frac{\partial}{\partial x}\right)^2 \phi + g \frac{\partial \phi}{\partial y} = 0 \Rightarrow \quad (2.6)$$

$$-w^2 \phi - 2i w U \frac{\partial \phi}{\partial x} + U^2 \frac{\partial^2 \phi}{\partial x^2} + g \frac{\partial \phi}{\partial y} = 0 \quad (2.7)$$

where :

$$w = w_0 - k U \cos(\theta)$$

and

$$k = \frac{w^2}{g}$$

The diffraction problem :

We know that :

$$\phi_0 = \frac{i g A}{w_0} \exp[K y - i k (x \cos(\theta) + z \sin(\theta) + i (w_0 - k U \cos(\theta) t)] \quad (2.8)$$

also, we want :

$$\nabla^2 \phi_A = \nabla^2 (\phi_0 + \phi_7) = 0 \Rightarrow \nabla^2 \phi_7 = 0 \quad (2.9)$$

boundary conditions (on body surface):

$$\frac{\partial \phi_A}{\partial n} = 0 \Rightarrow \frac{\partial (\phi_0 + \phi_7)}{\partial n} = 0 \Rightarrow \frac{\partial \phi_0}{\partial n} = -\frac{\partial \phi_7}{\partial n} \quad (2.10)$$

Therefore :

$$\frac{\partial \phi_7}{\partial n} \simeq -iw_0(n_y - in_z \sin(\theta)) * \exp[-ikx \cos(\theta) + iwt] \quad (2.11)$$

The form of this boundary condition suggests that the scattering potential can be expressed as :

$$\phi_7 = -iw_0(\psi_2 - i \sin(\theta) \psi_3) \exp[-ikx \cos(\theta) + iwt] \quad (2.12)$$

where the functions ψ_2 and ψ_3 satisfy the boundary conditions :

$$\left. \begin{aligned} \frac{\partial \psi_2}{\partial N} &= n_y \\ \frac{\partial \psi_3}{\partial N} &= n_z \end{aligned} \right\} \text{on the body surface} \quad (2.13)$$

Applying the free-surface condition :

$$\left(\frac{\partial}{\partial t} - U \frac{\partial}{\partial x}\right)^2 \phi + g \frac{\partial \phi}{\partial y} = 0 \Rightarrow \quad (2.14)$$

$$-w^2 \phi - 2iwU \frac{\partial \phi}{\partial x} + U^2 \frac{\partial^2 \phi}{\partial x^2} + g \frac{\partial \phi}{\partial y} = 0 \quad \text{on } y = 0 \quad (2.15)$$

on ϕ_7 gives the expression:

$$-w_0^2 \psi_j - 2iw_0U \frac{\partial \psi_j}{\partial x} + U^2 \frac{\partial^2 \psi_j}{\partial x^2} + g \frac{\partial \psi_j}{\partial y} = 0 \quad \text{on } y = 0 \text{ (j=2,3)} \quad (2.16)$$

Thus the potentials ψ_j can be regarded as forced-motion potentials, with oscillation occurring at the incident wave frequency w_0 , as measured in a fixed reference frame.

(In contrast with forced-motion potential ϕ_j , for which oscillation frequency is w , as measured in a moving reference frame).

2.3 Numerical method

To calculate the velocity potentials ϕ_j , the ship's hull was divided into segments. On each segment a constant velocity potential ϕ_j was assumed. Using Green's theorem :

$$\int \int_S (\phi_j \frac{\partial G}{\partial n} - G \frac{\partial \phi_j}{\partial n}) dS = -2\pi \phi_j(x, y, z)^1 \quad (2.17)$$

According to [17] the Green function for oscillatory motion in two dimensions, with infinite depth is given by :

$$G = [\log \frac{r}{r_1} - 2 \oint_0^\infty (k-1)^{-1} e^{-kY} \cos(kZ) dK] \cos(wt) - 2\pi e^{-Y} \cos(Z) \sin(wt) \quad (2.18)$$

where:

r, r_1 : radial distances from the source or its image to the field point.

w : radian frequency of motion

t : time

$$k = \frac{w^2}{g}$$

Y, Z : the nondimensionalized coordinates (by k) of the field point relative to the image source above the free surface.

Apart from the integral, all the terms and their derivatives are easy to calculate. The integral is defined in the Cauchy principal-value sense. It may be replaced by the real part of the complex function [16],[17] :

$$F(Z, Y) = \oint_0^\infty e^{-kY + ikZ} (k-1)^{-1} dk \quad (2.19)$$

Derivatives can be evaluated from the same function .

$$F_z = -iF - i(Y - iZ)^{-1} \quad (2.20)$$

$$F_y = -F - (Y - iZ)^{-1} \quad (2.21)$$

It may be proven that :

¹ $\frac{\partial \phi_j}{\partial n}$ on body surface is known.

$$F = e^{-Y+iZ} \int_{-Y+iZ}^{\infty} e^{-t} t^{-1} dt + \pi i e^{-Y+iZ} \quad (2.22)$$

or:

$$F = e^X * E_1(X) + \pi i e^X \quad (2.23)$$

where:

$$X = -Y + iZ$$

and

$$E_1(X) = \int_x^{\infty} e^{-t} t^{-1} dt \quad (2.24)$$

A series expansion for the above Green function is :

$$F(Z, Y) = e^x [-\gamma - \ln Z - \sum_{n=1}^{\infty} \frac{(-z)^n}{n \cdot n} + \pi \cdot i] \quad (2.25)$$

where $\gamma = 0.5772157...$ (Euler's constant)

This series is absolutely convergent.

Using Green's theorem to calculate the scattering potential ϕ_7 , we arrive at the following formula :

$$\sum_{k=1}^n \phi_k \frac{\partial G_{kl}}{\partial n} + \sum_{k=1}^n G_{kl} \frac{\partial \phi_k}{\partial n} = 2\pi \phi_l \quad (2.26)$$

where Green's function and its derivatives have been given above.

In matrix form :

$$(\phi_1 \frac{\partial G_{11}}{\partial n} + \phi_2 \frac{\partial G_{21}}{\partial n} + \dots + \phi_k \frac{\partial G_{k1}}{\partial n}) + (G_{11} \frac{\partial \phi_1}{\partial n} + G_{21} \frac{\partial \phi_2}{\partial n}) = 2\pi \phi_1 \quad (2.27)$$

$$(\phi_1 \frac{\partial G_{12}}{\partial n} + \phi_2 \frac{\partial G_{22}}{\partial n} + \dots + \phi_k \frac{\partial G_{k2}}{\partial n}) + (G_{12} \frac{\partial \phi_1}{\partial n} + G_{22} \frac{\partial \phi_2}{\partial n}) = 2\pi \phi_2 \quad (2.28)$$

$$(\phi_1 \frac{\partial G_{1k}}{\partial n} + \phi_2 \frac{\partial G_{2k}}{\partial n} + \dots + \phi_k \frac{\partial G_{kk}}{\partial n}) + (G_{1k} \frac{\partial \phi_1}{\partial n} + G_{2k} \frac{\partial \phi_2}{\partial n}) = 2\pi \phi_k \quad (2.29)$$

$$\begin{pmatrix} \frac{\partial G_{11}}{\partial n} - 2\pi & \frac{\partial G_{21}}{\partial n} & \dots & \frac{\partial G_{k1}}{\partial n} \\ \frac{\partial G_{12}}{\partial n} & \frac{\partial G_{22}}{\partial n} - 2\pi & \dots & \frac{\partial G_{k2}}{\partial n} \\ \dots & \dots & \dots & \dots \\ \frac{\partial G_{1k}}{\partial n} & \frac{\partial G_{2k}}{\partial n} & \dots & \frac{\partial G_{kk}}{\partial n} - 2\pi \end{pmatrix} \begin{pmatrix} \phi_1 \\ \phi_2 \\ \dots \\ \phi_k \end{pmatrix} = \quad (2.30)$$

$$= \begin{pmatrix} G_{11} \frac{\partial \phi_1}{\partial n} + G_{21} \frac{\partial \phi_2}{\partial n} + \dots + G_{k1} \frac{\partial \phi_k}{\partial n} \\ G_{12} \frac{\partial \phi_1}{\partial n} + G_{22} \frac{\partial \phi_2}{\partial n} + \dots + G_{k2} \frac{\partial \phi_k}{\partial n} \\ \dots \\ G_{1k} \frac{\partial \phi_1}{\partial n} + G_{2k} \frac{\partial \phi_2}{\partial n} + \dots + G_{kk} \frac{\partial \phi_k}{\partial n} \end{pmatrix} \quad (2.31)$$

Forces acting on the body :

Forces and moments acting on the body can be calculated by substituting the velocity potential in Bernoulli's equation. Thus, in linear terms we have :

$$p = -\rho \left(\frac{\partial \phi}{\partial t} + gy \right) = -\rho Re \left[\left(\sum_{j=1}^6 \xi_j \phi_j + A(\phi_0 + \phi_7) i w e^{iwt} \right) - \rho gy \right] \quad (2.32)$$

After integration over the hull surface we get :

$$\begin{pmatrix} F \\ M \end{pmatrix} = -\rho g \int \int_{S_B} \begin{pmatrix} \vec{n} \\ \vec{r} * \vec{n} \end{pmatrix} y dS \quad (2.33)$$

$$-\rho Re \left[\sum_{j=1}^6 i w \xi_j e^{iwt} \int \int_{S_B} \begin{pmatrix} \vec{n} \\ \vec{r} * \vec{n} \end{pmatrix} \phi_j dS \right] \quad (2.34)$$

$$-\rho Re \left[i w A e^{iwt} \int \int_{S_B} \begin{pmatrix} \vec{n} \\ \vec{r} * \vec{n} \end{pmatrix} (\phi_0 + \phi_7) dS \right] \quad (2.35)$$

or (using strip theory):

$$\sum_{j=1}^6 \xi_j (-c_{ij} + f_{ij}) + AX_i = -w^2 \sum_{j=1}^6 M_{ij} \Rightarrow \quad (2.36)$$

$$\sum_{j=1}^6 \xi_j [-w^2 (M_{ij} + a_{ij}) + iwb_{ij} + c_{ij}] = AX_i \quad (2.37)$$

where :

$$M_{ij} = \begin{pmatrix} m & 0 & 0 & 0 & mZ_G & -mY_G \\ 0 & m & 0 & -mZ_G & 0 & mX_G \\ 0 & 0 & m & mY_G & -mX_G & 0 \\ 0 & -mZ_G & mY_G & I_{11} & I_{12} & I_{13} \\ mZ_G & 0 & -mX_G & I_{21} & I_{22} & I_{23} \\ -mY_G & mX_G & 0 & I_{31} & I_{32} & I_{33} \end{pmatrix} \quad (2.38)$$

m: ship's mass

X_G, Y_G, Z_G : coordinates of the center of gravity

I_{ij} : moments of inertia

D : ship's displacement

$$\rho \int_{\Sigma} \phi_i n_j dl = a_{ij} + \frac{1}{i\omega} b_{ij} \quad (2.39)$$

$$c_{22} = \rho g S$$

$$c_{44} = \rho g S_{33} + \rho g D Y_B - m g Y_G$$

$$c_{45} = -g(\rho D X_B - m X_G)$$

$$c_{65} = -g(\rho D Z_B - m Z_G)$$

$$c_{66} = \rho g S_{11} + \rho g D Y_B - m g Y_G$$

For other values (i,j), $c_{ij} = 0$.

From the above equations we can define the ratio $\frac{\xi_i}{A}$ (i.e. the vessel's response per unit

wave amplitude). Replacing the ship's response and velocity potentials in eq. 2.1 we get the pressure distribution due to waves.

2.4 Program structure

The program built to calculate the hydrodynamic forces has the following structure :

1. Input data consists of the ship's speed and heading relative to the wave's front , wave frequency, and the ship's hull form.
2. The hull's geometry is read and panel information is generated (areas and direction cosines).
3. The solution of the radiation problem for sinusoidal motion of the ship with unit amplitude follows. The added mass (a_{ij}) and damping (b_{ij}) per station in heave, pitch, and sway is then calculated by summing up the velocity potentials (see eq. 2.39). For the calculations, the frequency of the encounter (frequency with which the ship meets the waves) is used. Frequency of encounter : $w = w_0 - kU \cos(\theta)$
4. The solution of the diffraction problem is similar to the above, except that the excitation frequency now is the natural frequency of the waves w_0 .
5. The matrix of equations of motion of the vessel is solved.
6. Having defined the motion for each panel of the ship's hull, the velocity potential of the ship is evaluated.
7. Finally, the sum of the induced and diffracted potentials is calculated.
8. According to the dynamic Bernoulli formula , the pressure distribution around the ship's hull is evaluated.

2.5 Results

The results acquired from the program are shown in the following figures.

- We notice that the higher the speed, the higher the amplitude of the heave motion of the vessel.
- When the vessel cruises at service speed, we observe two areas of large heave motion: one is found between the frequencies 0.6 and 0.7 [rad/sec] when the ship's heading is between 90^0 and 130^0 (beam seas) and the other is found at frequencies lower than 0.2 [rad/sec]. This corresponds to a wave length roughly equal to two times the beam of the ship for the first case, and two times the length of the ship (for heading waves) for the second one.

Potential flow theory gives accurate results for small wave heights and the ship's motions. On the other hand, the predicted high heaving amplitudes are higher than the actual ones, as we have a bare hull configuration (no fins) and we have considered inviscous flow (no damping due to viscosity). While investigating fatigue loads, the total error will be small, as the rate of occurrence of waves with large amplitude is small.

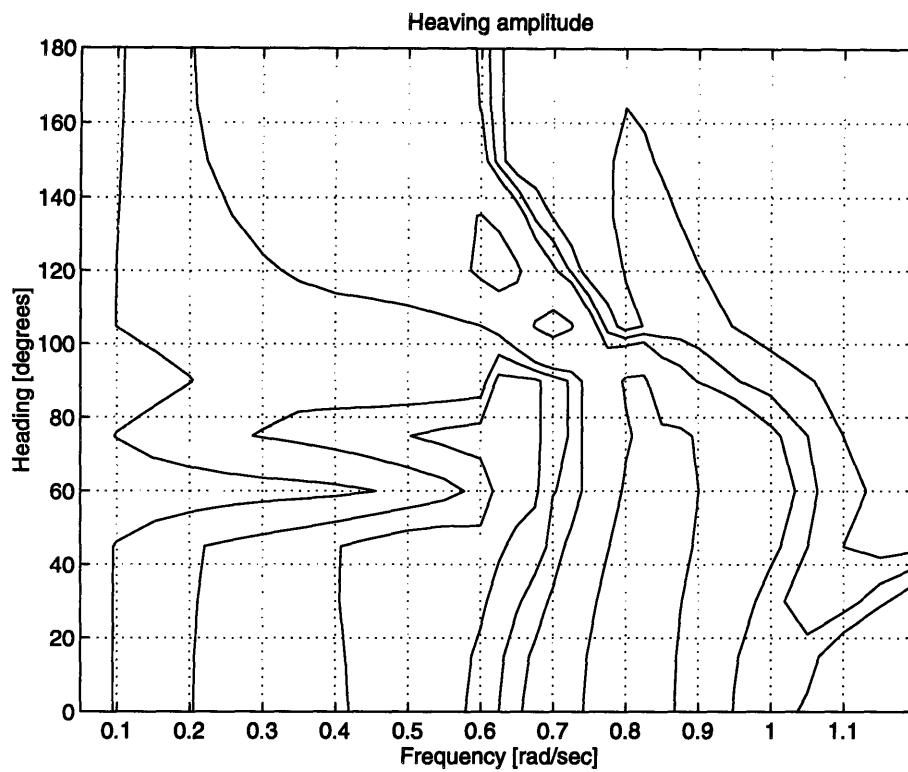


Figure 2-1: Heaving amplitudes for different headings-wave frequencies.

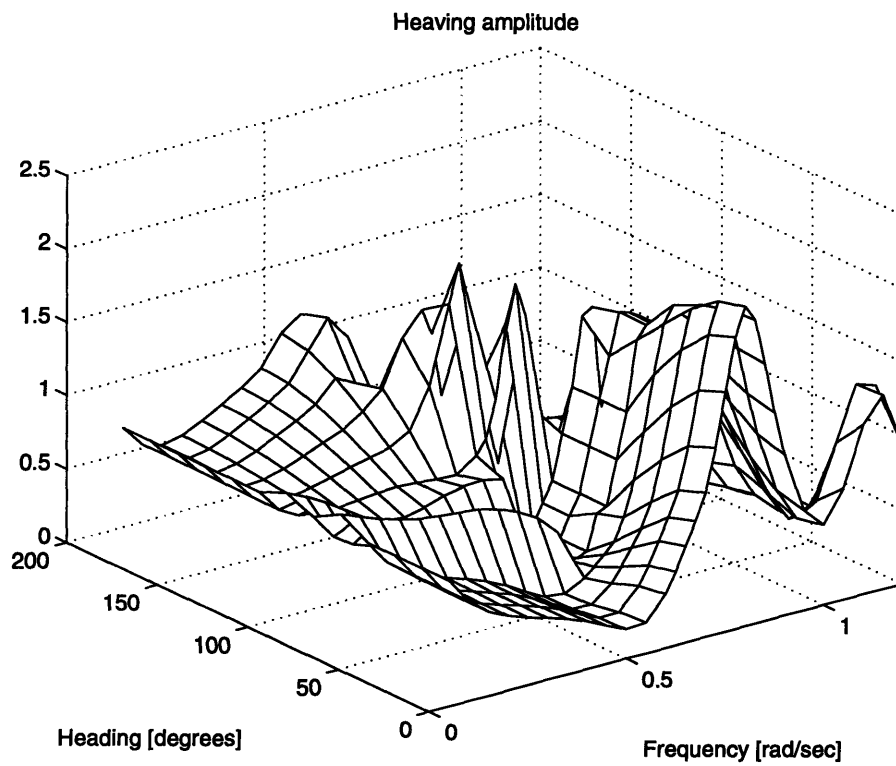


Figure 2-2: Heaving amplitudes for different headings-wave frequencies.

Chapter 3

Description of SWATH ship structure

3.1 Main configuration

The ship under investigation was designed similar to TAG-X [7], a SWATH vessel designed to assist hydro-acoustic research in the North Atlantic. Its principal characteristics (i.e. dimensions, materials applied and design loads) were used as guidelines. The main characteristics of the ship are the following (see fig. 3.1 for a general view):

- Displacement (tons) 4,000.0
- Overall length (ft) 282.0
- LBP (ft) 282.0
- Maximum breadth (ft) 82.0
- Lower length (ft) 292.0
- Lower hull max. width (ft) 23.0
- Lower hull max. depth (ft) 16.5
- Strut length (ft) 238.0

- Strut thickness at midsection (ft) 9.0
- Strut separation (ft) 69.0
- Box length (ft) 238.0
- Box overall breadth (ft) 48.0
- Box height (ft) 11.0
- Box clearance (ft) 12.0
- Draft at DWL (ft) 21.5

The ship structure was to be constructed entirely of ordinary steel. However, many classification societies recommend the insertion of high strength steel in areas of known stress concentrations (e.g. the box-haunch-strut intersections near major transverse bulkheads).

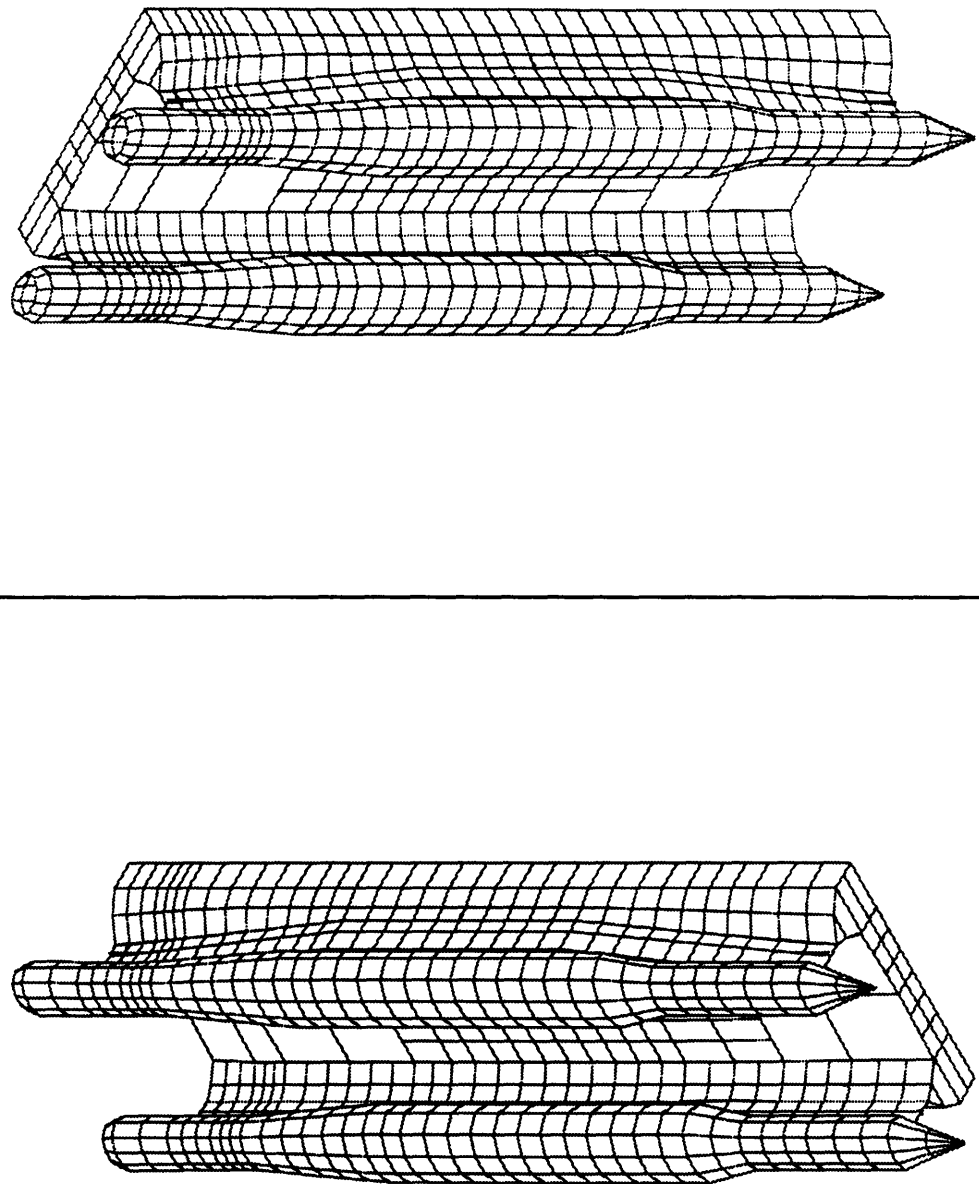
In figures 3.3, 3.4 and 3.5, we see the structural design at three transverse sections (at $L/4$, $L/2$ and $3L/4$) and five longitudinal sections. In fig. 3.5 the first /upper number shows the plate thickness (in inches) and the second number shows the code number for the stiffeners (see App. A). Figures from A to E correspond to the following cross-sections :

- A:Centerline
- B:Hull
- C:Platform
- D:Knee
- E:Pin

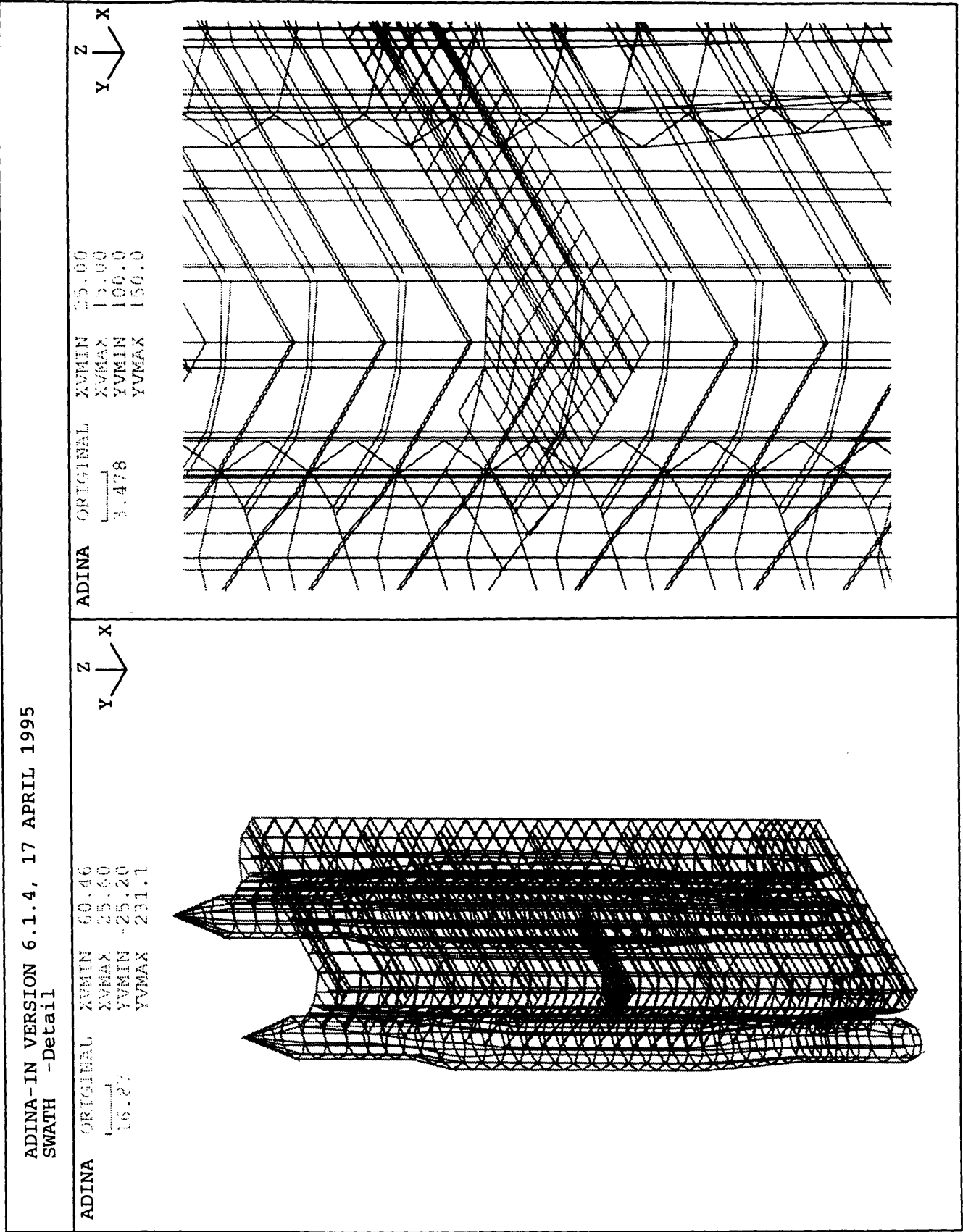
According to these designs, longitudinal girders on 8.00 feet spacing in the box area and 24.00 inch transverse frame spacing were installed. Girders were also placed in the shell of the struts (both inboard and outboard).

In the following finite element analysis, the ship was modeled with a coarse mesh. The point of interest was modeled with a finer mesh (see fig 3.2). Boundary conditions for the

area of interest (haunch) were obtained by applying the prescribed pressure distribution on the full structure. This is a common practice for determining detailed stress results for a component of a large structure [9],[13].

[illegible]

34



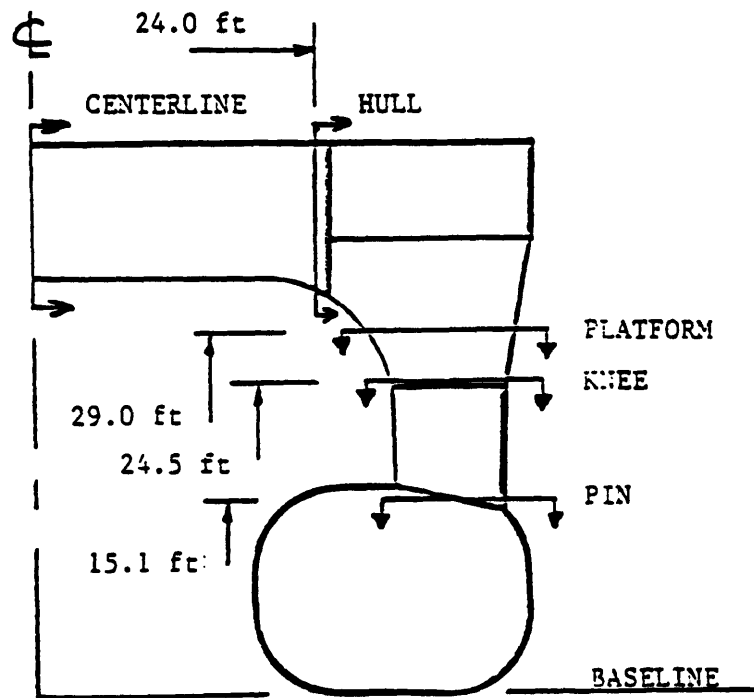
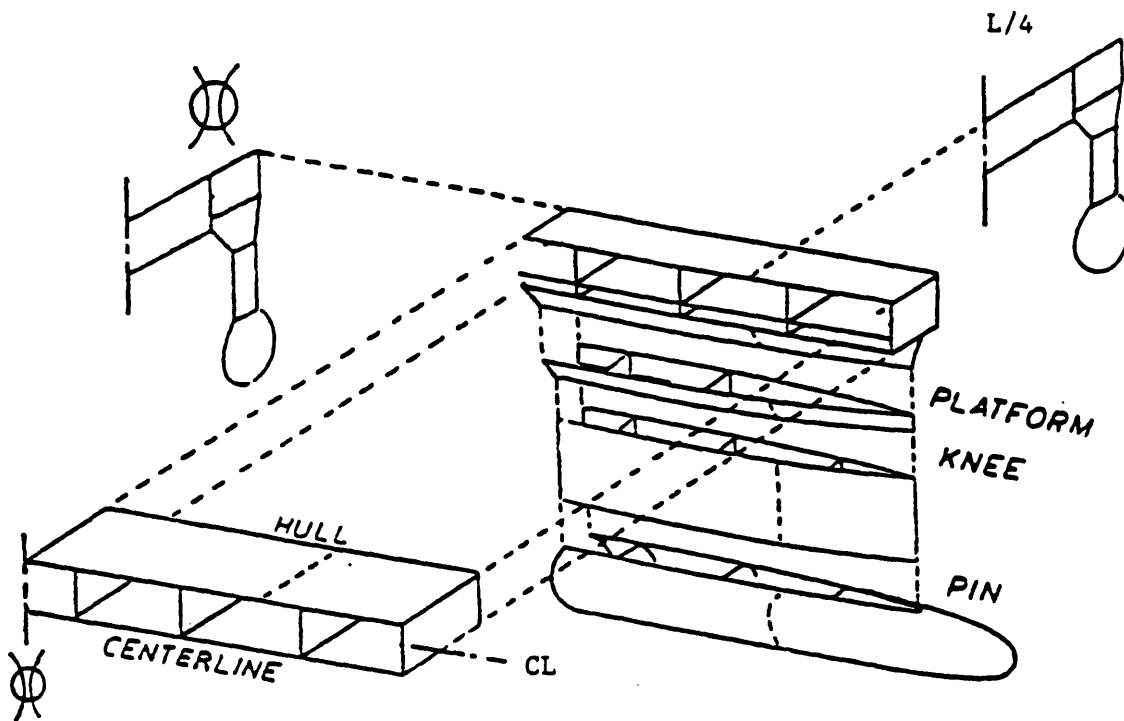


Figure 3-3: Locations of Longitudinal and Transverse cross sections for the design of ship structure.

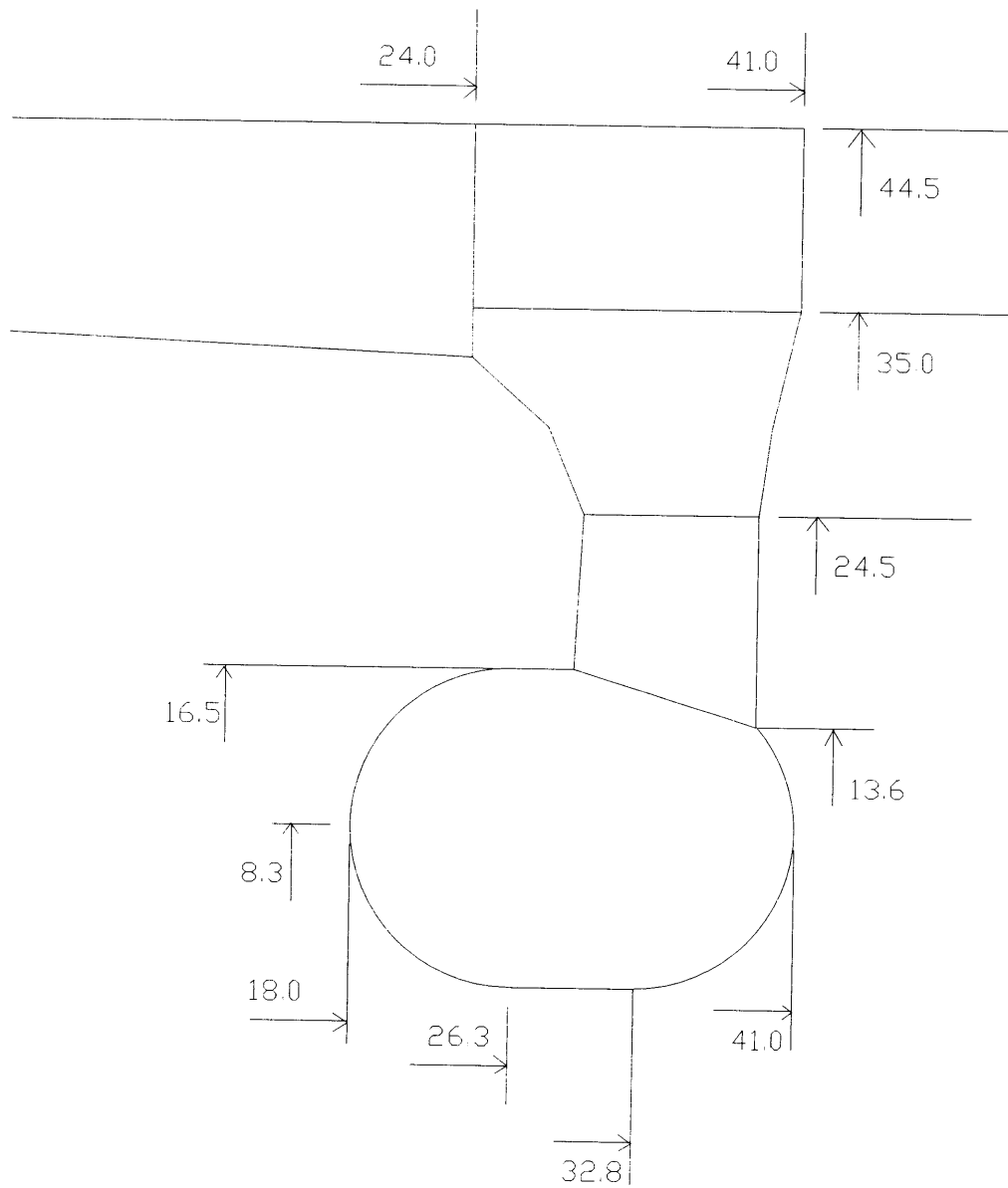


Figure 3-4: Midsection at $L/2$

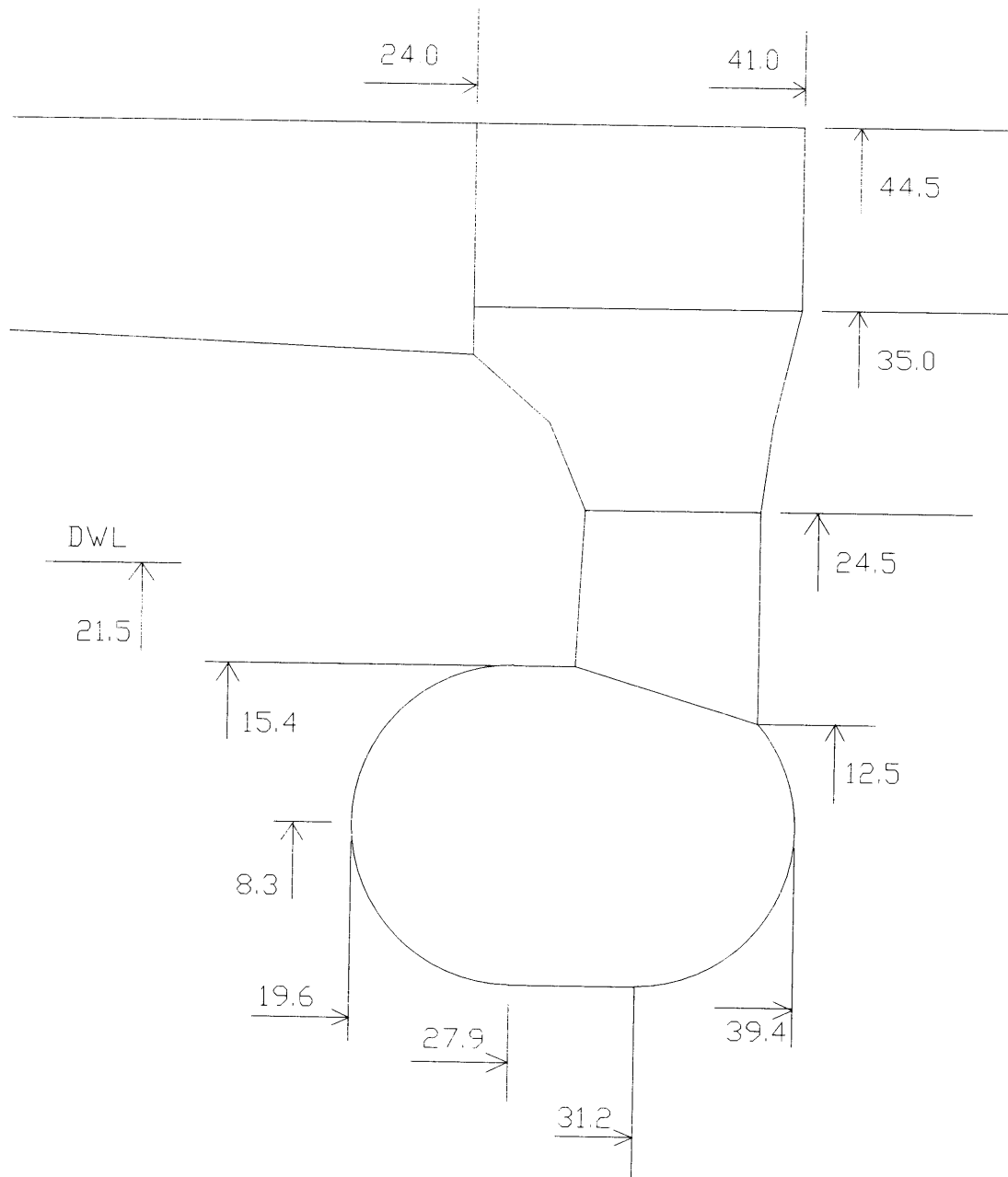


Figure 3-5: Midsection at $L/4$ and $3L/4$

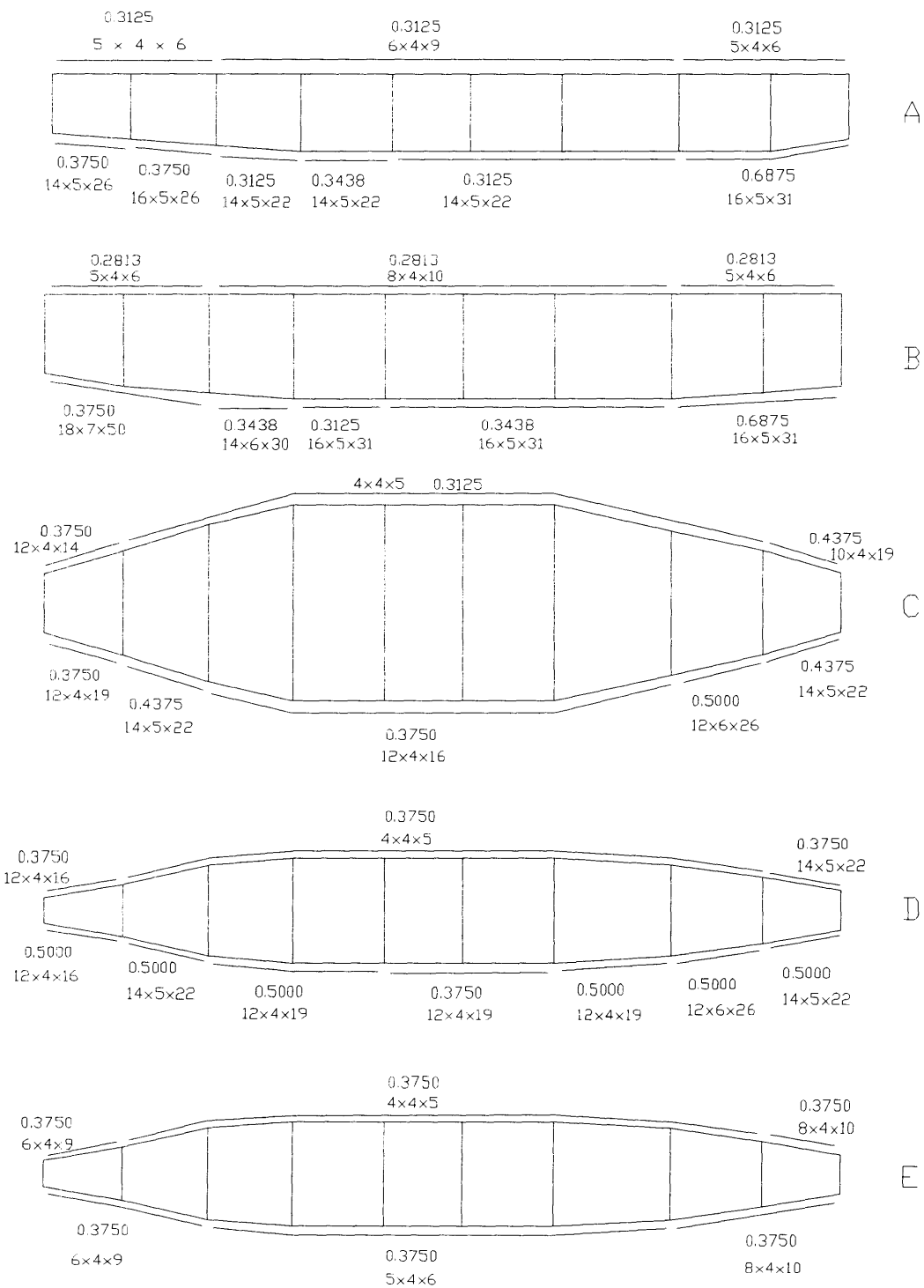


Figure 3-6: Diagram of plates and stiffeners.

3.2 Finite element investigation

The following steps were taken to determine the impact of geometry design and of mesh on stress evaluation.

- Change of the strut form so that no discontinuity on the shell surface is present. Discontinuities cause high local stresses, and to define their exact magnitude a very fine mesh is needed.
- Increase of the radius of the haunch to 4 feet and 9 feet successively.
- Use of a finer mesh (more elements and more nodes per element).

The above steps were examined for a ship heading of 90^0 , ship speed 27 ft/sec (service speed) and a wave frequency of 334.47 [deg/sec].

The results taken for each step are given in Table 3.1 (stresses were examined on the upper corner of the notch, where the maximum stress has been observed during a loading cycle):

Step	$\sigma_{effective}$	Phase
Initial geometry	7,350.12	150^0
R=4 ft	5,362.16	150^0
R=9 ft.	2,452.83	180^0
Finer mesh	2,398.74	180^0

Table 3.1: Impact of design on stress concentration.

From the above table, we conclude that increasing the radius of the notch causes a large drop in the maximum stress. Also, a further increase on the number of elements / nodes per element gives a difference of 2.25%. This difference is not large enough to justify the time and memory required for the solution of such a fine mesh.

In the following figures, the constructed mesh for each case (fig. 3.7, 3.8, 3.9 and 3.10) as well as stress concentration in the discontinuities of the midsection (fig. 3.11) are shown.

For the reasons stated above (smaller stress concentration, less time, and memory requirements) the mesh shown in fig. 3.9 was selected for further analysis. Multiple runs were made

ADINA-IN VERSION 6.1.4, 15 MAY 1995
Mesh no. 1

ADINA ORIGINAL XVMIN 8.000
XVMAX 41.00
YVMIN 24.50
YVMAX 36.16

Y
X

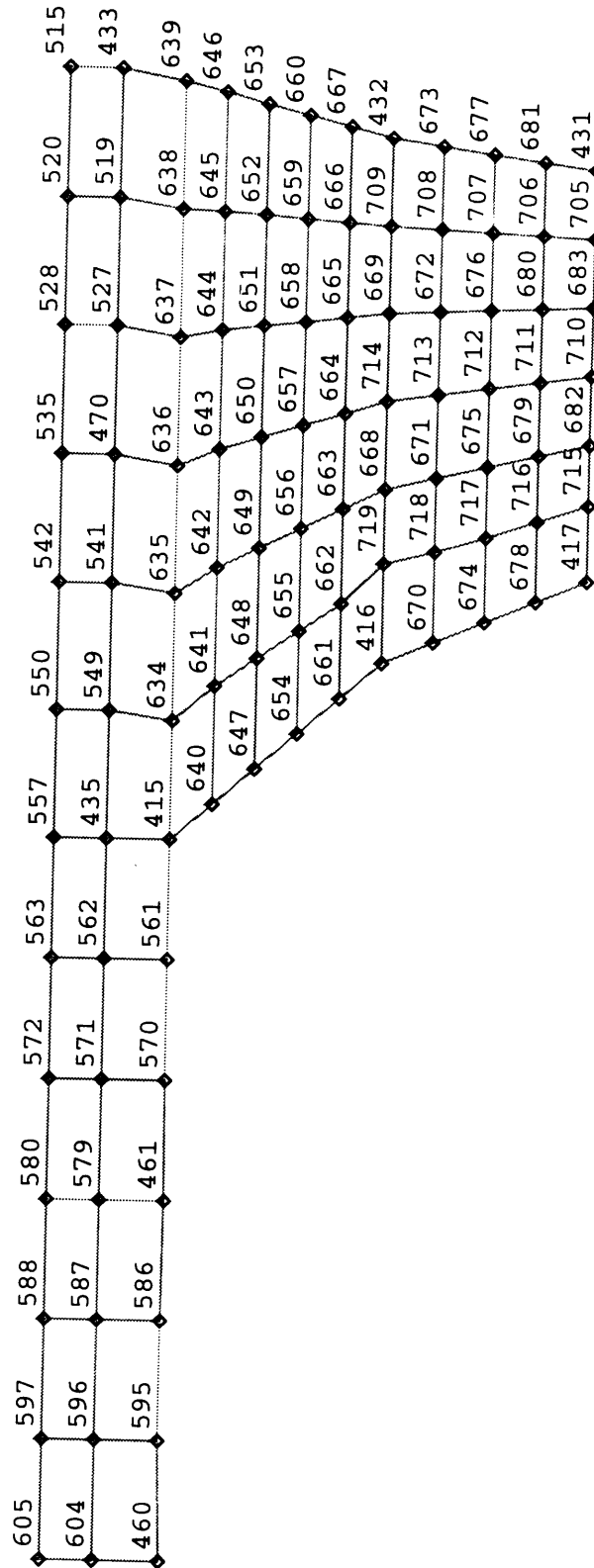


Figure 3-7: Midsection (notch design).

ADINA-IN VERSION 6.1.4, 15 MAY 1995
 Mesh no. 2

ADINA ORIGINAL XVMIN 8.000
 XVMAX 41.00
 YVMIN 24.50
 YVMAX 36.16

Y
 X

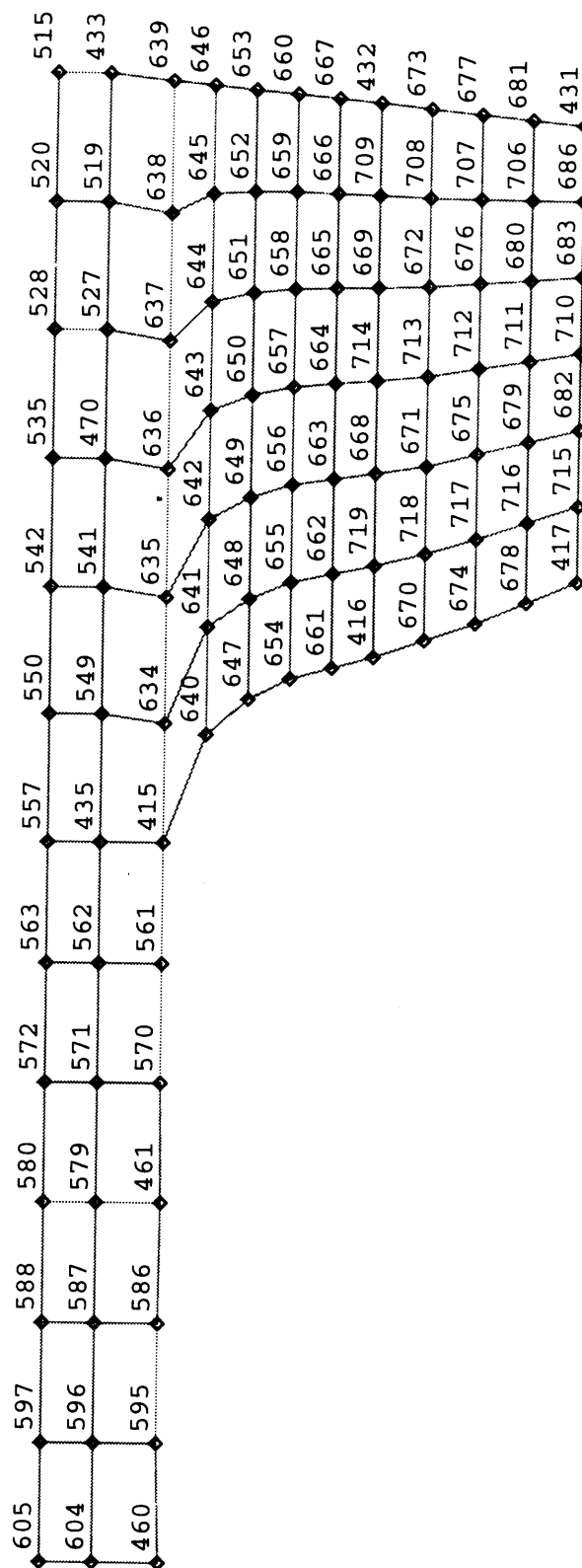


Figure 3-8: Midsection (Radius =4 ft).

ADINA-IN VERSION 6.1.4, 15 MAY 1995
 Mesh no. 3

ADINA ORIGINAL XVMIN 8.000
 XVMAX 41.00
 YVMIN 24.50
 YVMAX 36.16

Y
 X

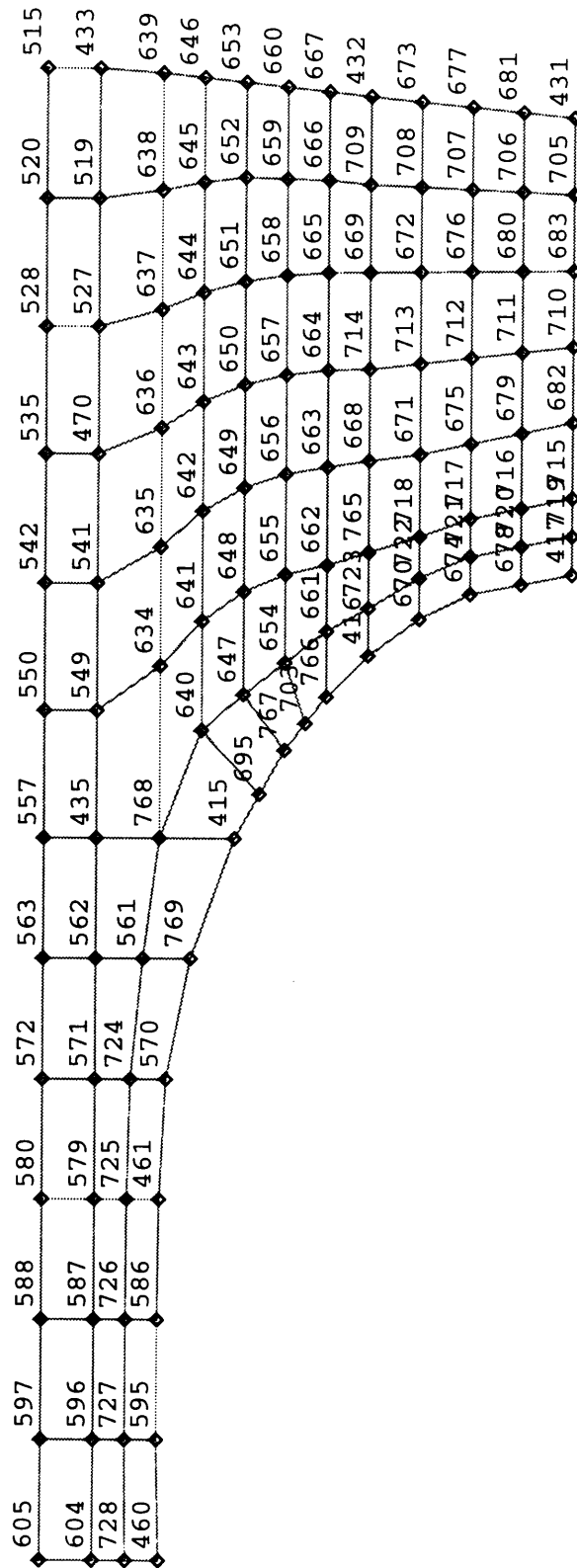


Figure 3-9: Midsection (radius=9 ft).

YVXIN	2	0.00
YVMAZ	4	1.00
YVMIN	5	4.50
YVMAZ	5	5.16

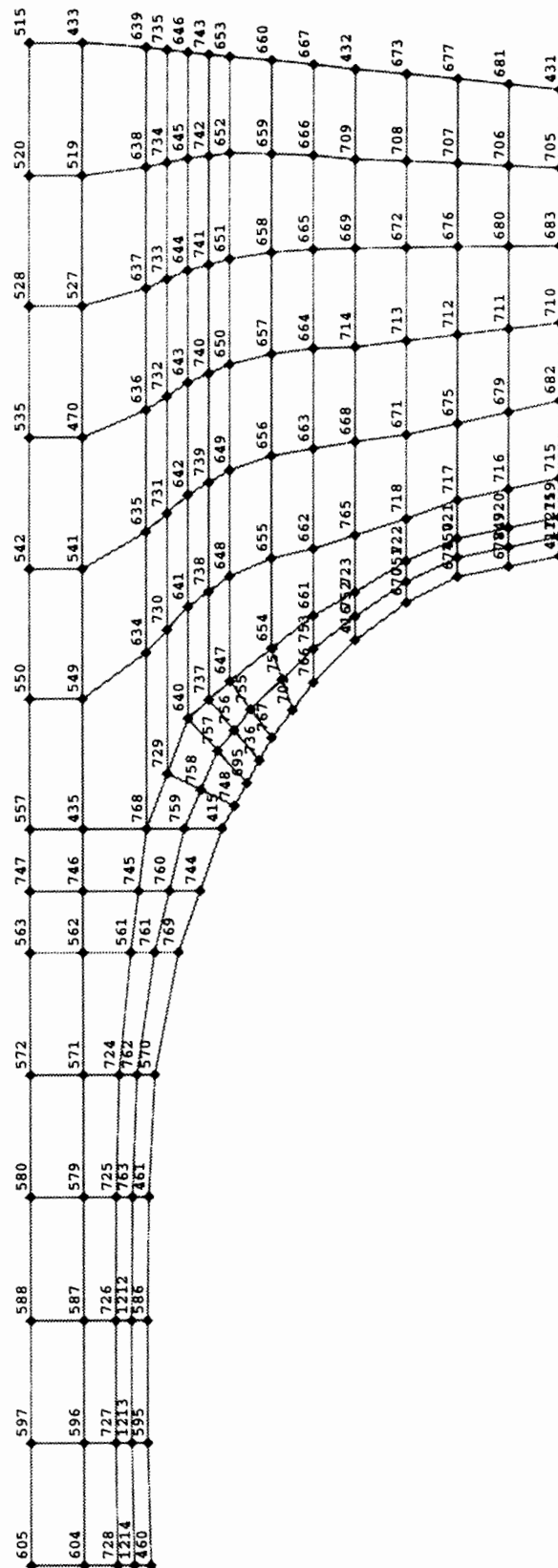


Figure 3-10: Midsection (finner mesh).

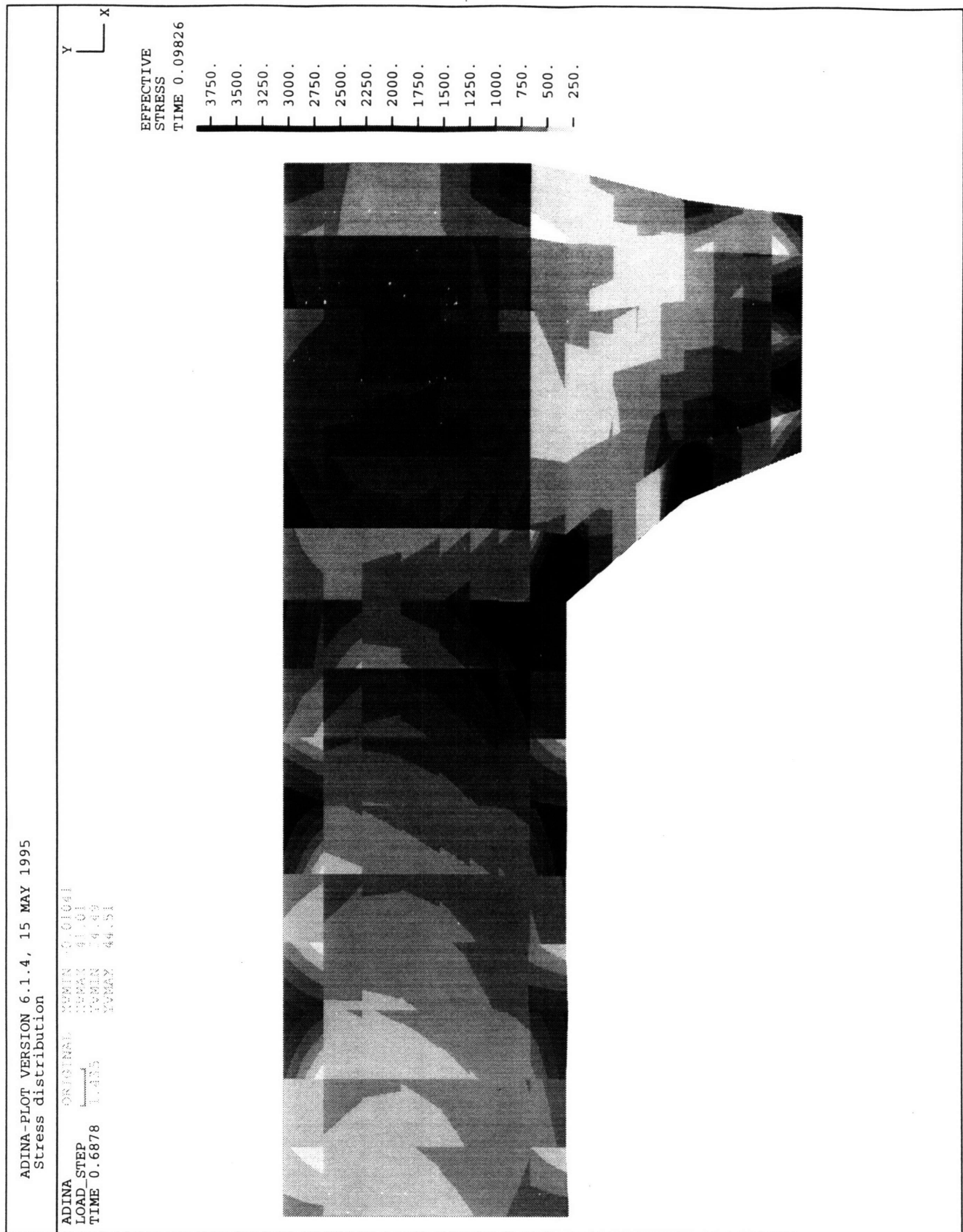


Figure 3-11: Stress distribution on mid-section.

for different ship's headings and wave frequencies. The results obtained are shown in fig. 3.12, 3.13, 3.14 and 3.15.

Large stresses are observed for wave frequencies between 275 and 375 [deg/sec] and zero heading. This is caused by the large heaving motion which occurs when the ship travels at this course in this sea state.

Another stress peak is observed at a heading of 90^0 and a wave frequency of 260 [deg/sec]. In such a sea state, wave lengths equal to 2 times the beam of the ship result in the formation of high stresses. A slight change in course and/or wave frequency greatly diminishes the stresses.

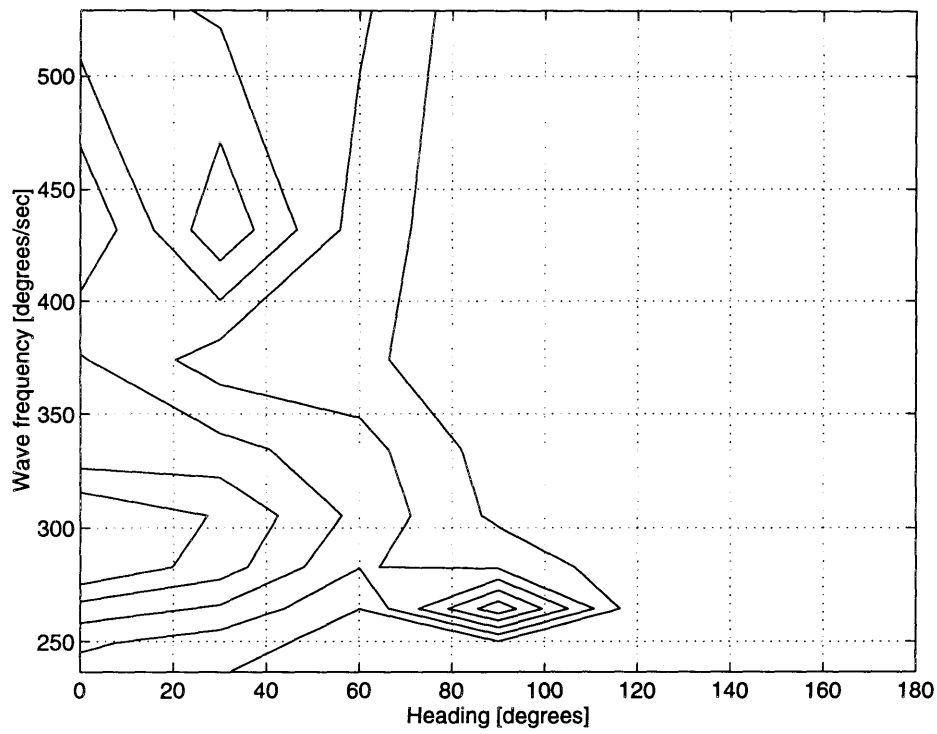


Figure 3-12: Stress σ_{xx} (transverse direction).

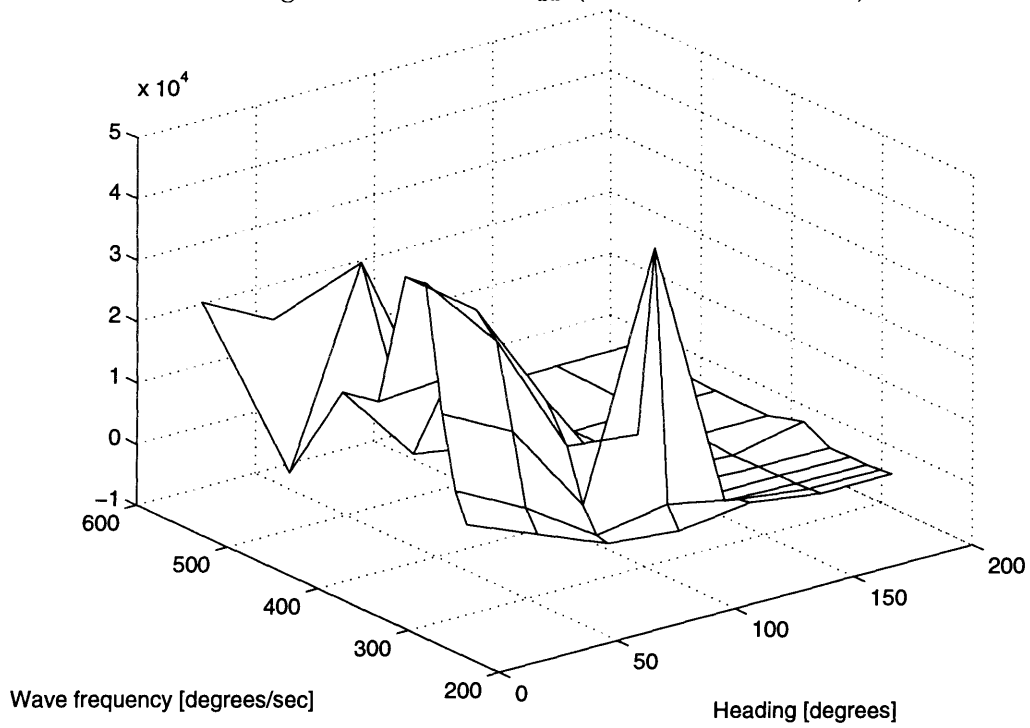


Figure 3-13: Stress σ_{xx} (transverse direction).

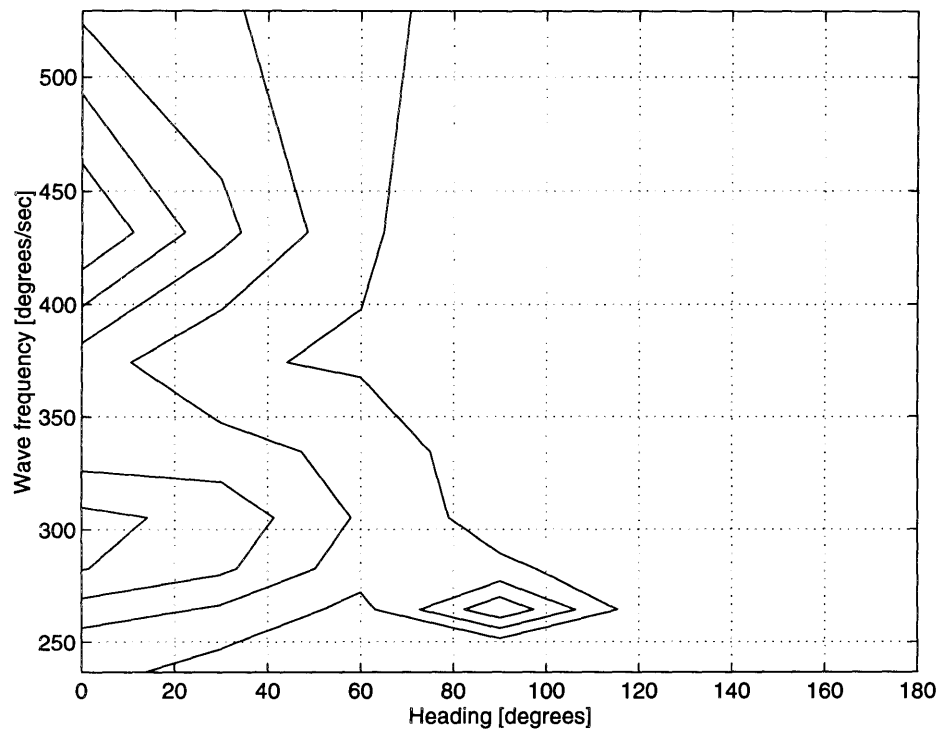


Figure 3-14: Stress σ_{vv} (vertical direction).

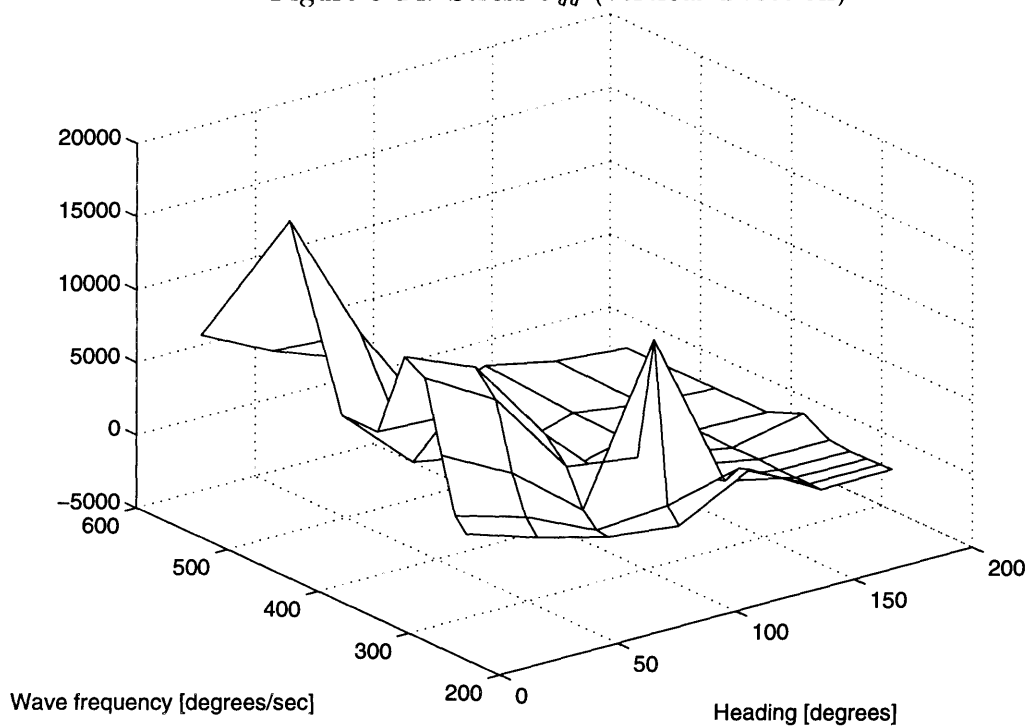


Figure 3-15: Stress σ_{yy} (vertical direction).

3.3 Fatigue loads.

As we saw in the previous section, wave induced loads were imposed on the struts and lower hulls. The load produces a force perpendicular to the plane of the struts. This normal force produces transverse bending in the box and struts and torsion (about the vertical axis) in the struts.

The effects of the loading differ for varying sea conditions. In beam seas, maximum normal forces and relatively small torsional effects are observed. In bow and quartering seas normal forces are reduced and torsional loads are increased.

Classification societies do not require any specific structural reinforcement for the combined lateral and torsional loads produced in oblique seas, as designing the ship structure for the lateral loads of beam seas provides adequate strength.

As in conventional monohull ships, large bending moments occur in the longitudinal direction (hogging and sagging). Hence, longitudinal framing is necessary in the ships' structural design. In SWATH ships, which have small waterplane area (cross sectional area cutting through the struts), the stresses due to hogging and sagging are minimized. On the contrary, the normal load on the struts causes large transversal bending moments. Therefore, the hull girder structure on SWATH ships should be designed for both transversal and longitudinal bending.

Consideration should also be given to stresses generated from the normal loads on the struts and the ship's dead load weight. Although the resultant stresses are small compared to the transverse bending, they produce shear stresses in the transverse bulkheads. The thickness of the bulkheads must be such that they withstand these shear stresses.

Finally, during the design phase of the structure, special consideration is given to secondary loads (i.e. loads that affect the structure in the immediate vicinity of their area of application). These are hydrostatic loads, flooding or damage loads, deck and platform live loads, dead loads, and wet deck slamming pressures. The size and location of live loads for decks and platforms are estimated based on past experience.

Using the ADINA code, the maximum stresses in the haunch, when the ship's speed is 27 ft/sec (service speed), were found to be the following:

heading: 0 degrees

freq.	1.4690	1.1995	1.0388	0.9291	0.8481	0.7852	0.7345	0.6925	0.6569
txx	28000	6900	24000	25200	47500	48000	28000	16500	11800
tyy	8900	19500	7800	7800	13800	13000	8200	4500	3600
txy	-15000	-35000	-13800	-13800	-25000	-25000	-14700	-8700	-6300

heading 30 degrees

freq.	1.4690	1.1995	1.0388	0.9291	0.8481	0.7852	0.7345	0.6925	0.6569
txx	22000	38000	10800	26000	39000	35500	22000	10500	7100
tyy	6500	10500	3300	7600	11800	10200	5700	3100	2050
txy	-11200	-18500	-6200	-13800	-20500	-17800	-9800	-5200	-3650

heading 60 degrees

freq.	1.4690	1.1995	1.0388	0.9291	0.8481	0.7852	0.7345	0.6925	0.6569
txx	16500	11300	8900	18300	2100	15200	6800	2900	2450
tyy	4700	3550	2450	5200	5800	4300	1850	890	780
txy	-8300	-6300	-4450	-9000	-11700	-7500	-3350	-1450	-1180

heading 90 degrees

freq.	1.4690	1.1995	1.0388	0.9291	0.8481	0.7852	0.7345	0.6925	0.6569
txx	1480	1000	1180	2550	4800	13900	45500	4800	1370
tyy	410	420	340	570	1210	3600	12200	1250	235
txy	-720	-680	-530	-1150	-2250	-6400	-22000	-2350	-470

heading 120 degrees

freq.	1.4690	1.1995	1.0388	0.9291	0.8481	0.7852	0.7345	0.6925	0.6569
txx	1550	1050	950	980	1100	900	1200	2500	2800
tyy	600	420	350	280	220	160	215	600	630
txy	-1000	-780	-630	-550	-430	-320	-430	-1180	-1190

heading 150 degrees

freq.	1.4690	1.1995	1.0388	0.9291	0.8481	0.7852	0.7345	0.6925	0.6569
txx	1800	1300	1250	650	800	900	850	1070	1200
tyy	530	330	230	150	210	120	120	115	100
txy	-950	-570	-390	-330	-330	-240	-260	-310	-290

heading 180 degrees

freq.	1.4690	1.1995	1.0388	0.9291	0.8481	0.7852	0.7345	0.6925	0.6569
txx	1900	1300	1250	3000	740	760	780	1000	1205
tyy	105	110	115	1150	185	75	80	135	160
txy	-330	-250	-280	-2000	-285	-175	-180	-270	-345

3.3.1 Fatigue fracture.

In steel and other metals, a fluctuating stress can initiate microscopic cracks which gradually increase in size until, after a large number of cycles, the cracks have become so large that fracture occurs. Fatigue fracture is entirely distinct from static tensile fracture [4].

In fatigue the most important parameter is the stress range, which is the total (peak to peak) variation in the cyclic stress. Since fatigue damage is cumulative, the occurrence of fracture depends on the magnitude and duration (number of cycles) of the individual cyclic loads which act on the structure throughout its life. For an individual cyclic load of constant amplitude (S) the number of cycles (N) which lead to fatigue fracture has been established experimentally for each type of steel and other materials.

This information is usually presented in “S-N diagrams” (see fig. 3.16) in which the horizontal distance to the sloping line is the fatigue life (number of cycles to failure) at that level of S for a certain type of structural specimen [12]. Each line is obtained by testing to failure a series of identical structural specimens at different ranges of S and then performing linear regression analysis on a log-log plot of the data, with a 95% confidence limit. Thus each line (or “S-N” curve, as it is commonly called) represents an exponential relationship of the form :

$$S_N = (C/N)^{1/m} \Rightarrow \log S_N = \frac{1}{m} \log C - \frac{1}{m} \log N$$

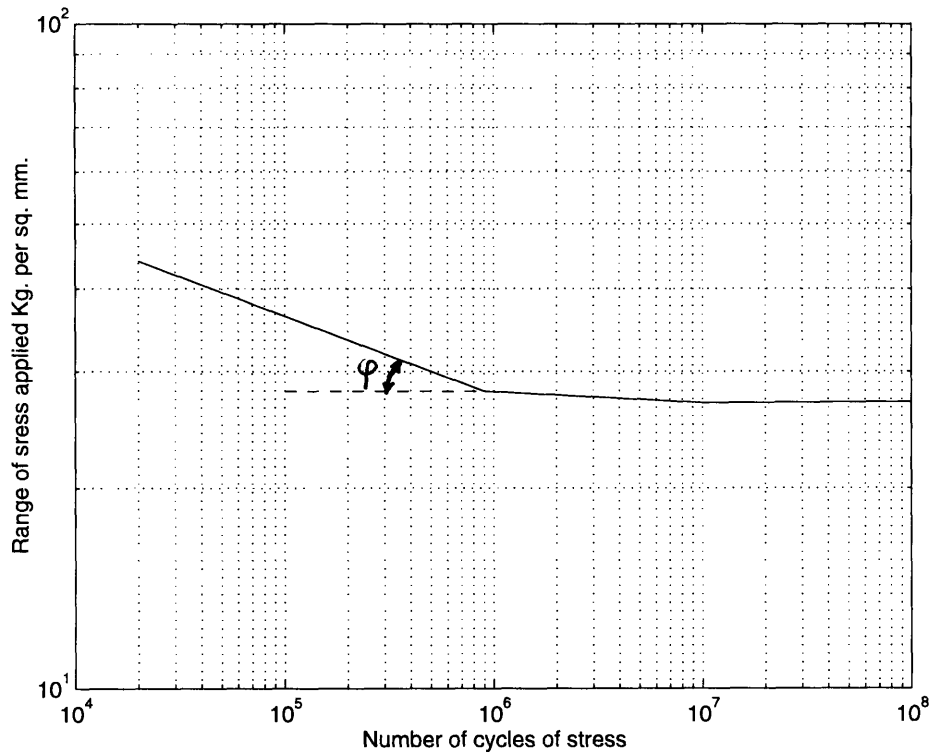


Figure 3-16: “S-N” curve for annealed medium carbon steel.

where:

N : number of cycles to failure for a constant amplitude stress range S_N .

$1/m$: the tangent of the angle ϕ .

S_N : the constant amplitude stress range for failure after N cycles.

For most materials there is a threshold level of stress range S_0 below which fatigue damage does not occur , regardless of the number of cycles. This is commonly referred to as the fatigue limit.

In a ship structure there are three main sources of cyclic stress : wave induced loads, especially bending on the hull girder, and mechanical sources such as the engine and the propellers. The number of wave bending cycles in a ship’s life (20 years) is of the order of 10^8 ¹.

¹During 20 years, by assuming an average wave period 7 s we find:

$$N = \frac{\text{years} \cdot \text{days} \cdot \text{hours} \cdot \text{seconds}}{\text{average wave period}} = \frac{20 * 365 * 24 * 3600}{7} = 0.9 \cdot 10^8$$

The method we are going to use to deal with fatigue is based on fatigue tests together with the hypothesis of linear damage accumulation (Miner's rule). According to this hypothesis the total fatigue life under a variety of stress ranges is the weighted sum of the individual cycles at constant S , as given by the S-N curves, with each being weighted according to the fractional exposure to that level of stress range. To apply this hypothesis the long-term distribution of stress range is replaced by a stress histogram, consisting of a convenient number of stress cycles n_i . The constraint against fatigue fracture is then expressed in terms of a nondimensional damage ratio n_L :

$$\sum_{i=1}^b \frac{n_i}{N_i} < n_L$$

where

b : the number of stress blocks

n_i : number of stress cycles in stress block i

N_i : number of cycles to failure at constant stress range S_i

n_L : limit damage ratio

The limit damage ratio n_L depends on the maintainability, that is, the possibility for inspection and repair, as well as the importance of the particular structural detail. For vital structural elements which are exposed to seawater a typical value of n_L is 0.3 if there is good access and maintainability and 0.1 if not.

3.3.2 Accumulative fatigue load calculation

To calculate the accumulative fatigue load, the following steps were followed:

- Calculation of the amplitude of stress variation for different headings and wave frequencies and for unit height wave (1 foot).
- Evaluation, for each wave frequency, of the resultant stress for different wave heights as well as the number of cycle loading over the ship's life (for that specific frequency).

H_s [ft]	Time period [sec]														
	1	2	3	4	5	6	7	8	9	10	11	12	13	14	15
3	59	9	0	0	0	0	0	0	0	0	0	0	0	0	0
4	403	212	8	0	0	0	0	0	0	0	0	0	0	0	0
5	1061	1233	146	6	0	0	0	0	0	0	0	0	0	0	0
6	1569	3223	831	85	4	0	0	0	0	0	0	0	0	0	0
7	1634	5106	2295	481	57	3	0	0	0	0	0	0	0	0	0
8	1362	5814	3896	1371	315	39	2	0	0	0	0	0	0	0	0
9	982	5284	4707	2406	898	207	27	2	0	0	0	0	0	0	0
10	643	4102	4456	2960	1564	571	136	20	2	0	0	0	0	0	0
11	395	2846	3531	2976	1879	950	347	88	15	2	0	0	0	0	0
12	232	1821	2452	2163	1696	1069	528	197	54	11	2	0	0	0	0
13	132	1098	1543	1437	1228	885	533	261	101	30	7	1	0	0	0
14	74	634	901	849	748	575	387	226	111	45	15	4	1	0	0
15	41	355	497	458	398	309	217	138	78	39	16	6	2	0	0
16	22	194	263	231	191	142	98	64	39	22	11	5	2	1	0
17	12	105	135	110	84	58	37	23	14	8	5	2	1	0	0
18	7	56	67	50	35	21	12	7	4	2	1	1	0	0	0
19	4	30	33	22	13	7	4	2	1	1	0	0	0	0	0
20	2	16	16	10	5	2	1	0	0	0	0	0	0	0	0
21	2	17	15	7	3	1	0	0	0	0	0	0	0	0	0

Table 3.2: Wave spectrum of North Atlantic.

- Accumulation of the ratios of number of cycle loading for a specific stress over the total number of cycles that cause failure (under this stress).

The number of cycles for each frequency/amplitude may be evaluated from table 3.2

Knowing the probability of occurrence for each frequency and wave amplitude (North Sea spectrum), we may calculate the stress distribution over the life of the ship².

The nondimensional damage ratio n_L is found to be 0.02 (inside classification society norms).

²See Appendix C for the calculations.

3.4 Natural frequencies

One of the first questions put before naval architects is the determination of the values of the natural frequencies of the ship girder's free vibrations according to various modes.

The knowledge of natural frequencies helps us to define the response of the structure on impact loads (due to high amplitude waves). Also, by comparing the ship's natural frequencies with the frequencies of the excitation loads (such as those caused by propeller's and main engine's vibrations) it gives a first approximation on potential problems due to high amplitude response to them.

The calculation methods used till now are based on Bernoulli's hypothesis, that a ship can be considered as a beam; thus the stresses appearing in different structural elements are proportional to the distance of this element to the neutral axis which passes through the gravity center of the surface of working elements.

This hypothesis assumes that the transverse plane sections remain plane during the deformation of the assembly and do not suffer any local deformations. This hypothesis is very doubtful when applied to a structure as complex as that of a monohull ship, and surely cannot be applied to a SWATH ship, the form of which can hardly be considered a beam ³.

Concerning monohull ships, the notions of the efficiency of the working section and the equivalent (fictive) inertia of the section were introduced to overcome the above difficulties.

The same approximations cannot be used for SWATH ships due to their complex geometry. Instead, a finite element analysis to calculate their natural frequencies is necessary.

The ADINA code was used to evaluate the natural frequencies of the SWATH ship.

The results obtained are the following :

³Monohull ships, in contrast with SWATHs, do possess two dimensions , height and breadth, which are very small in respect to the third one (i.e. the length).

Mode Number	eigenvalue	natural frequency [rad/sec]	frequency [Hz]
1	1.00000E-10	1.00000E-05	1.59155E-06
2	1.00000E-10	1.00000E-05	1.59155E-06
3	1.00000E-10	1.00000E-05	1.59155E-06
4	2.34490E-10	1.53131E-05	2.43715E-06
5	3.69027E-10	1.92101E-05	3.05738E-06
6	8.71724E-10	2.95250E-05	4.69905E-06
7	1.50406E+03	3.87822E+01	6.17238E+00
8	1.96975E+03	4.43818E+01	7.06359E+00
9	2.35626E+03	4.85413E+01	7.72558E+00

The first 6 modes have zero frequency as they correspond to the six rigid body modes of the free body.

The lowest natural frequency (7th mode) is more than four times higher than the wave frequencies for which high amplitude waves occur. Therefore, the loading of the ship structure for these wave frequencies should be considered as static (see also [19], p.525).

In fig. 3.17 we can see the grid's deformation due to modes 7,8 and 9.

ADINA-PLOT VERSION 6.1.4, 26 APRIL 1995
 MODES 7,8 AND 9

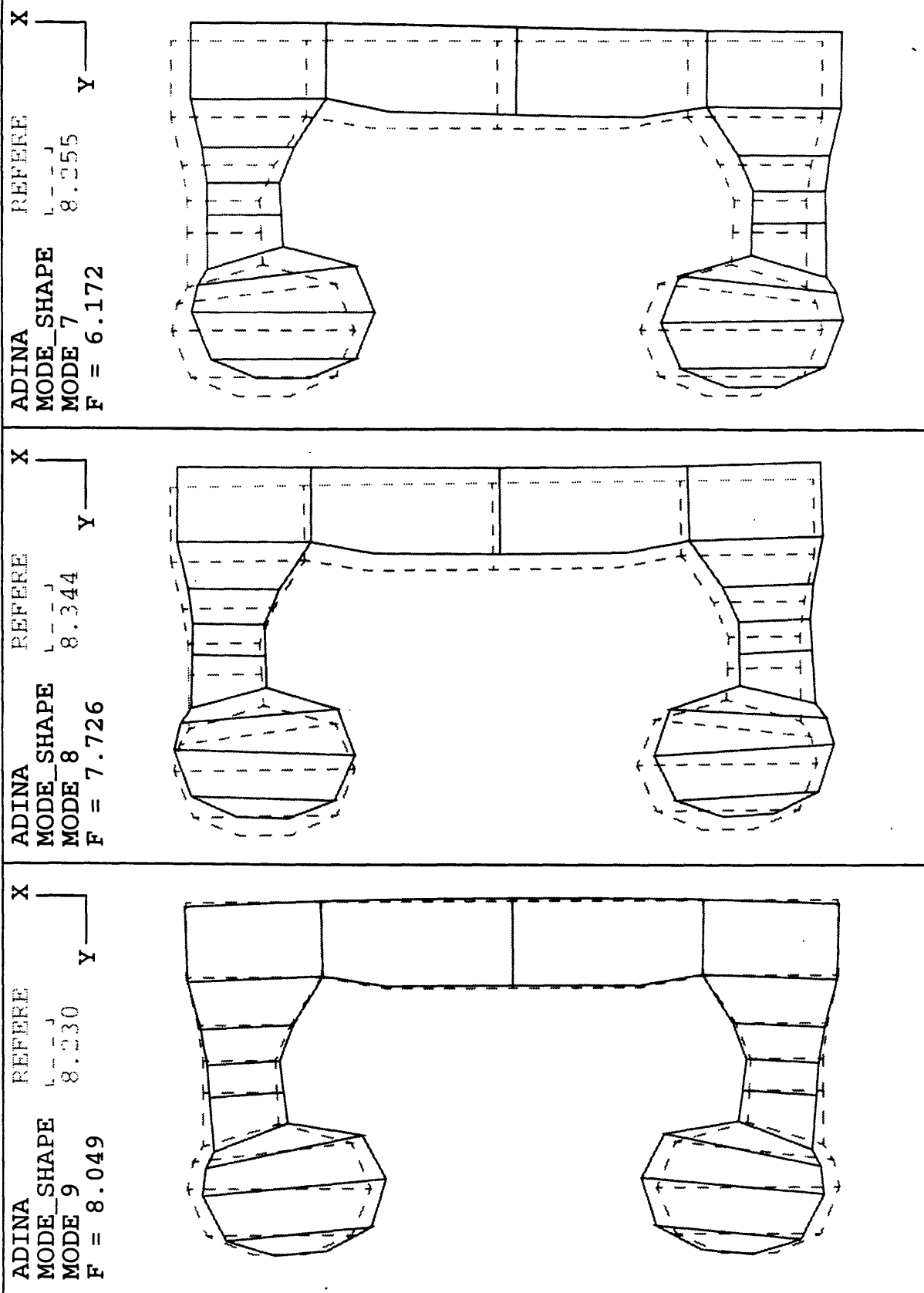


Figure 3-17: Natural frequencies, modes 7,8 and 9.

Chapter 4

Propeller vibrations

4.1 Procedure of vibration's measurement

Upon delivery from the shipyard and during sea trials, measurements of vibrations are obtained. Measurements are obtained in both loading conditions (loaded and ballast) and in different locations (different distances on the deck from ship's stern). It should be noted that, from past experience, moving forward from aft, the hull pressure decreases very slowly. For a tanker of 550,000 dwt (401 m - 1315 ft L_{bp}), on the ship's centerline and at a distance of about one propeller diameter forward of the propeller, pressure fluctuations of 800 millibars (mb) maximum were still measured in very light ballast (with the propeller tip just under water surface), while maximum pressure amplitude just above the propeller disc was 1110 mb [15].

4.2 Structure configuration

In order to do the following investigation, I assumed the shaft mounting to be similar to TAGOS-19 (see fig. 4.1). In addition, I designed the two identical propellers which would be mounted on the vessel, one on each lower hull. These propellers were designed so as to meet the requirements of stress and cavitation. They were optimized for maximum efficiency at service speed (18 knots). Their characteristics are the following :

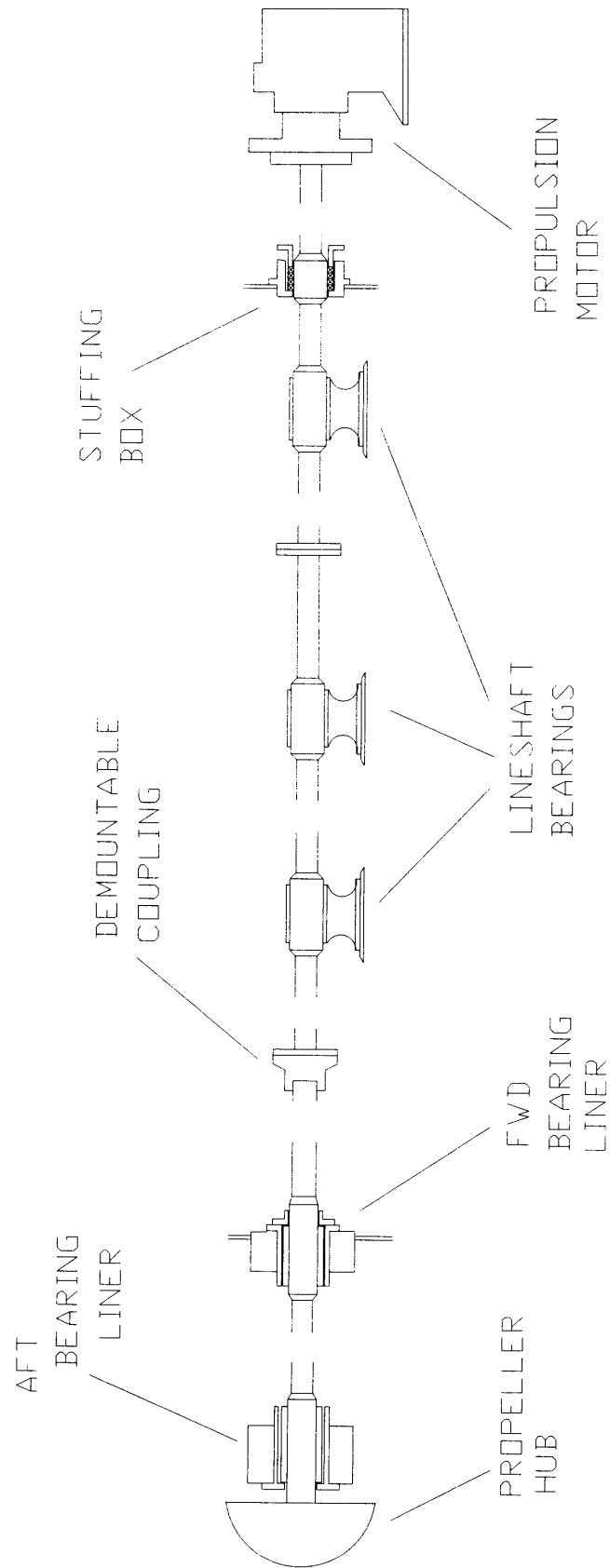


Figure 4-1: Shafting arrangement.

- Hub diameter : 3 ft
- Propeller diameter : 15 ft.
- Number of blades : 5
- Required power at maximum speed : 26,543.59 HP
- Required thrust at maximum speed : 176,226.63 lbf
- RPM (max. speed): 200

Table 4.1: Propeller description.

The choice of a 5 bladed propeller instead of a 4 bladed one was taken in accordance with the smoothness of the functioning of the propeller. The higher the number of blades, the lower are the excitation forces. A counter - rotating propeller would almost eliminate the vibrational forces but it would present the disadvantage of high drag (small efficiency) due to its larger hub. The designed propeller has the following geometry:

R/R_0	Radius	Chord Length	thickness	camber
0.2	18.00	45.79	8.3880	1.2936
0.25	22.50	41.99	7.9020	1.0932
0.3	27.00	41.13	7.4160	1.0591
0.4	36.00	40.55	6.4620	1.0541
0.5	45.00	40.48	5.5080	1.0310
0.6	54.00	40.37	4.5540	0.9758
0.7	63.00	39.55	3.6000	0.8906
0.8	72.00	37.42	2.6280	0.7683
0.9	81.00	31.93	1.6740	0.5822
0.95	85.50	25.25	1.2060	0.4187
1.0	90.00	0.36	0.7200	0.0000

4.3 Propeller forces

The PLL code was used for the calculation of the forces acting on the propeller's shaft. Wake data was assumed similar to TAGOS-19. The wake velocity profile may be seen in fig. 4.2, 4.3 and 4.4. We observed the sudden drop in velocity due to struts and aft fins.

As mentioned in section 1.2, propeller vibrations were due to two groups of excitation forces : hull pressure forces and bearing forces.

Hull pressure forces depend on the cavitation and hull geometry. In this case, the hull pressure forces may be assumed negligible for the following reasons:

- Since the shaft depth and the propeller diameter are both large, thus leading to low revolutions per minute (RPM) and high efficiency of the propellers, the extent of the cavitation is small.
- The Swath's lower hull geometry is such that there are no hull plates on the top of the propeller, the position where the largest amplitude vibrations are observed on monohull ships.(see fig. 1.2)

For the calculation of bearing forces, several runs were made. In each run, the wake was uniform and the velocity profile similar to the one the propeller "sees " at different angles.

For each one of the above runs, forces on chordwise strips of blades were evaluated. Adding up the forces on each strip, we calculated the force on each blade (see fig. 4.5). Adding up the forces on each blade (the perpendicular components only) for all angles, the total excitation force was extracted (see fig. 4.6). We may observe that although there is a drop in velocity (and consequently on blade loading) just behind the aft fins, the result is smoothed-out due to the rest of the blades. The same does not happen when a blade passes behind the strut. The velocity drop covers a wider angle, therefore producing an unstabilized force.

The higher amplitude was observed forward and aft of the bulkhead at amidships (see fig 4.7). By studying the two figures we note that the stiffeners diminish the vibration amplitude in their locality, which was expected. For the same reason, the amplitude of vibration is negligible close to the joints of the deck with the bulkheads.

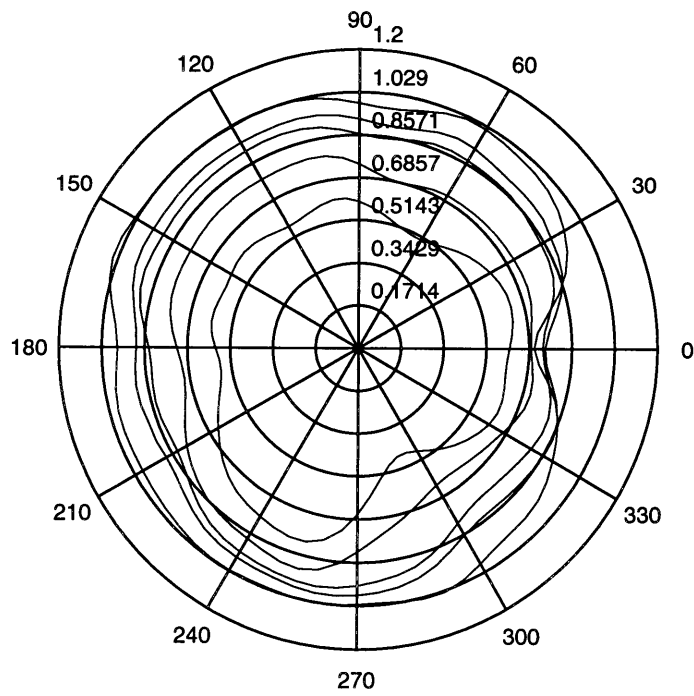


Figure 4-2: Axial wake velocities.

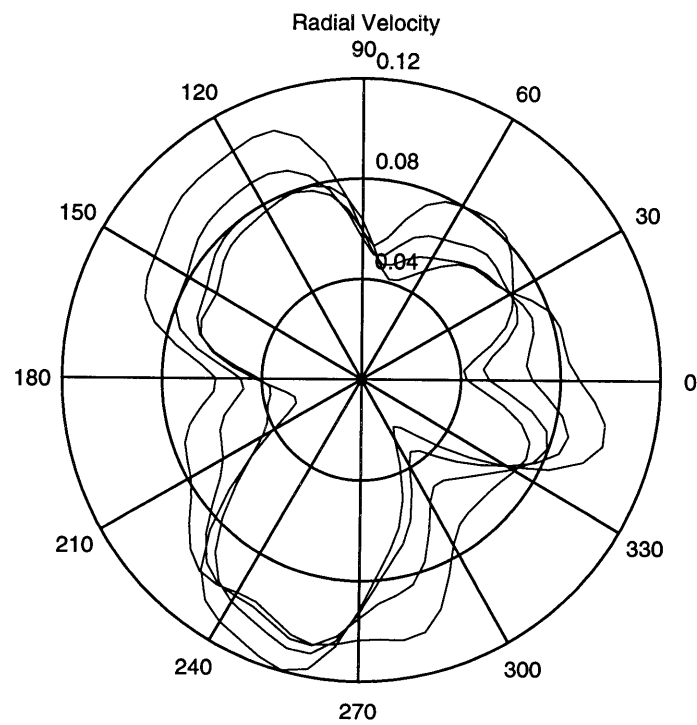


Figure 4-3: Radial wake velocities.

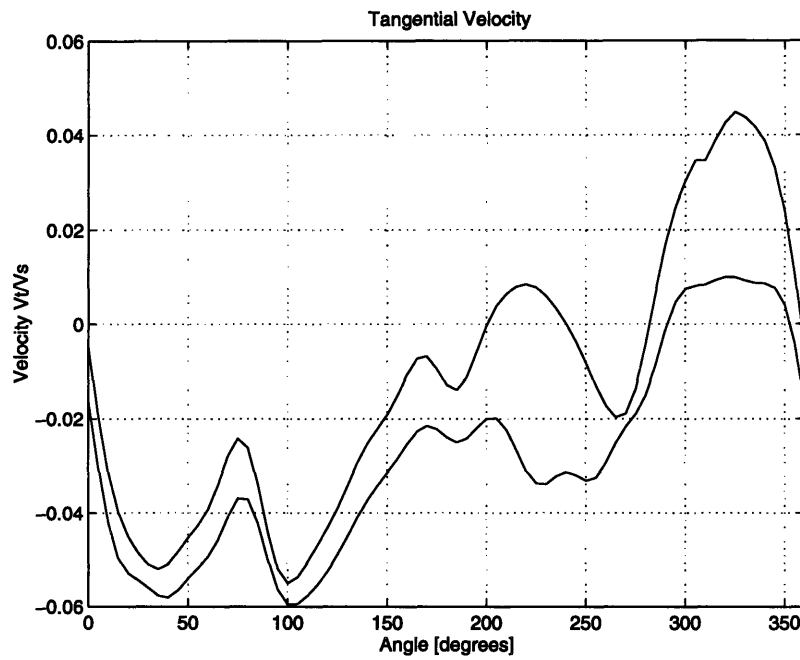


Figure 4-4: Tangential wake velocities.

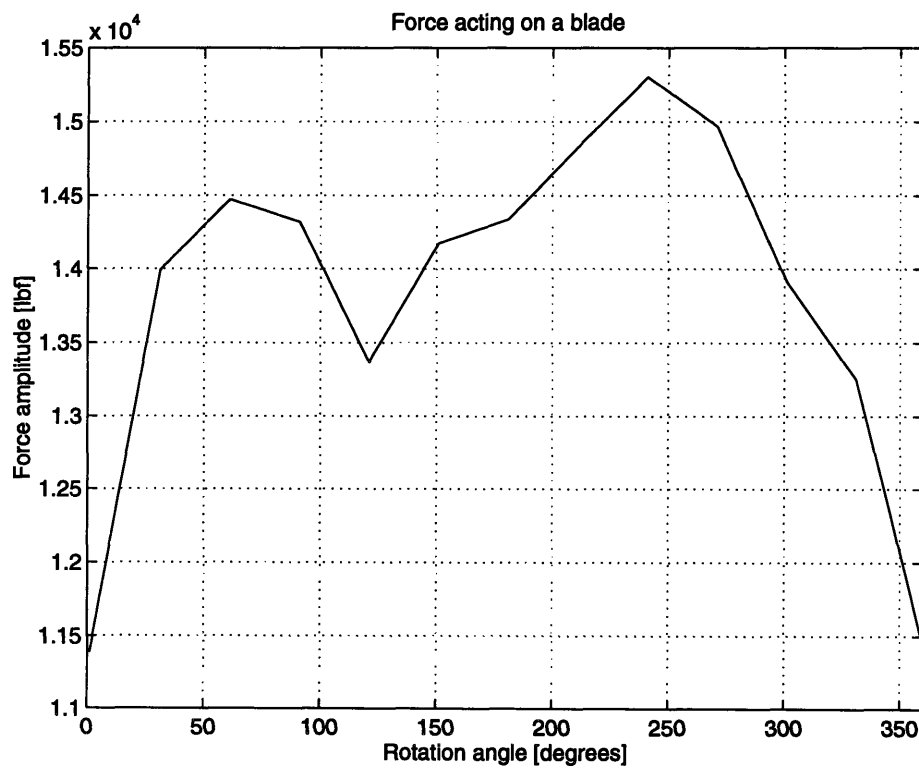


Figure 4-5: Blade load for each rotation angle.

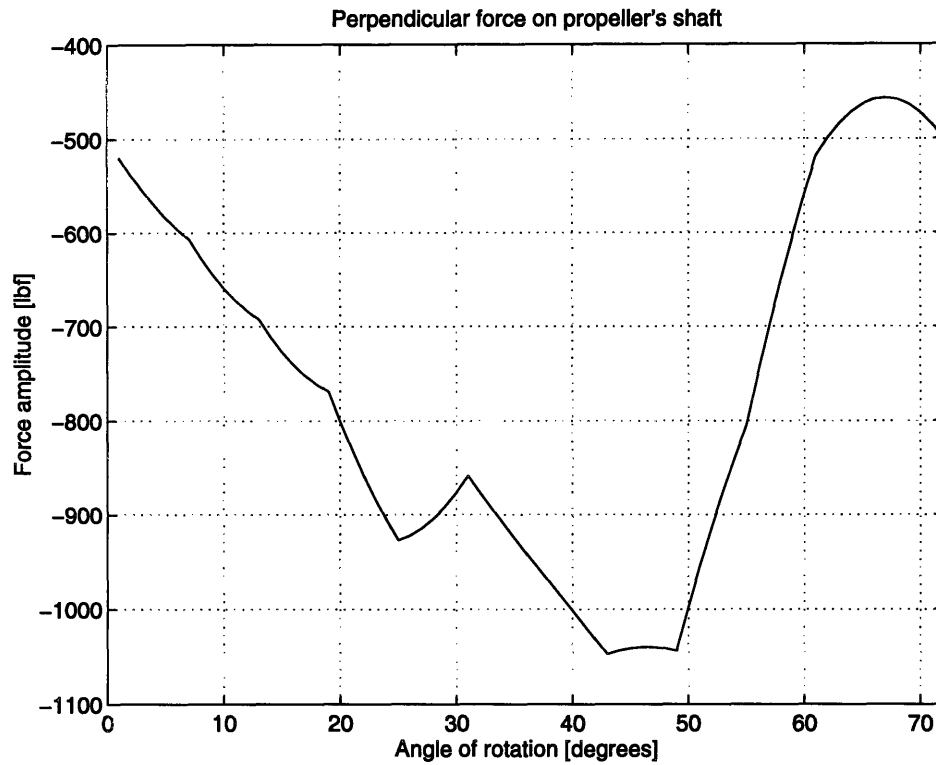


Figure 4-6: Total perpendicular force acting on propeller's shaft.

4.3.1 Results.

Following the directions of ISO 9000 for ship's vibration, a chart was traced. According to this graph, the vibration amplitude for the abovementioned location of maximum displacement is within limits.

ADINA-PLOT VERSION 6.1.4, 24 APRIL 1995
UPPER DECK DISPLACEMENT DUE TO PROPELLER VIBRATION

ADINA	ORIGINAL	DEFORME	Z	Y	X
LOAD_STEP	11.22	0.00018			
TIME 0.05000					
ADINA	ORIGINAL	DEFORME	Z	Y	X
LOAD_STEP	8.445	0.00018			
TIME 0.05000					

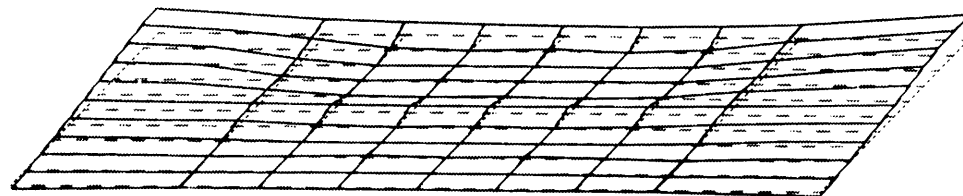
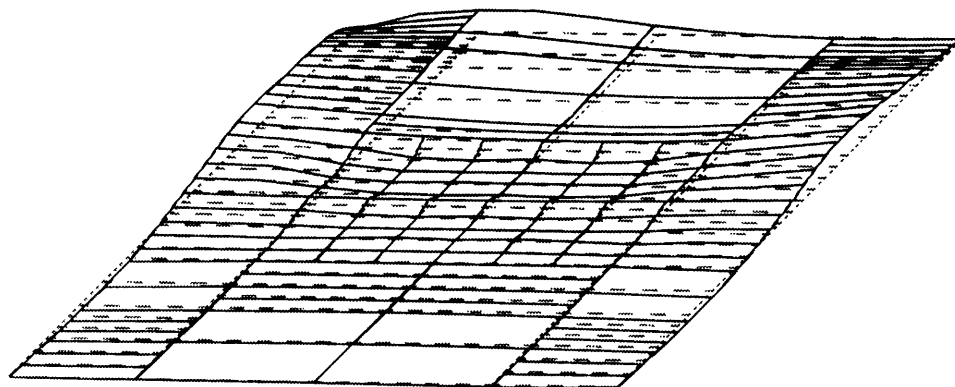
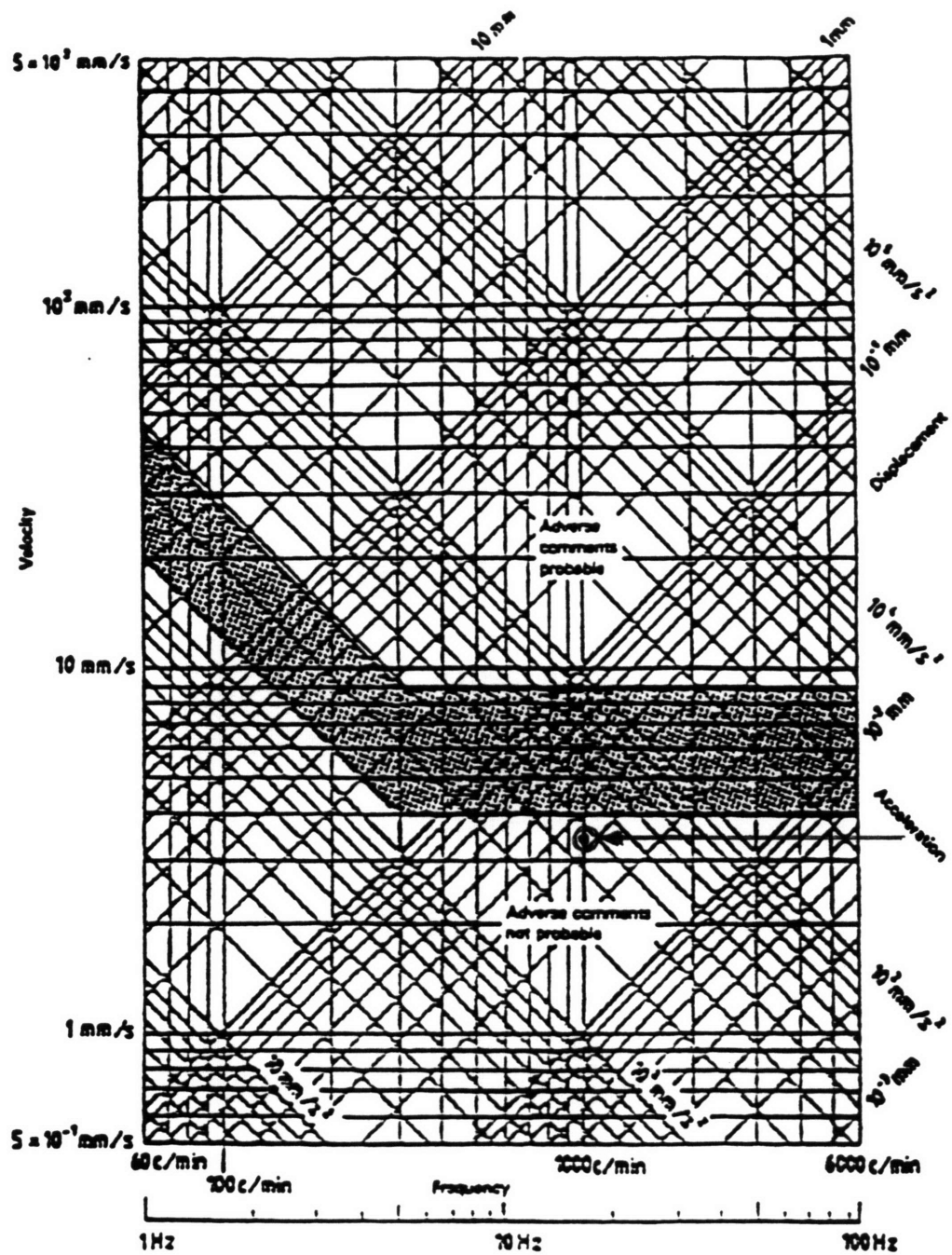


Figure 4-7: Deformation of upper deck due to propeller vibrations.



Curve	Frequency range	
	1 to 5 Hz	5 to 100 Hz
Upper	Peak acceleration ¹⁾ = 235 mm/s ²	Peak velocity ¹⁾ = 9 mm/s
Lower	Peak acceleration ²⁾ = 125 mm/s ²	Peak velocity ¹⁾ = 4 mm/s

Figure 4-8: ISO Amplitude Evaluation Guidelines.

Chapter 5

Conclusions

During the vibration analysis several aspects of SWATH's ships characteristics were considered and discussed: the behavior of the vessel in different sea states, both in terms of motions and stresses; natural frequencies of excitation in which irregular waves may excite the ship's structure; propeller forces due to non-uniform wake flow in which the propeller is obliged to work; and finally, the structure's response due to the excitation by the propeller forces.

In more detail:

In Chapter 2 a code was built to calculate in the ship's motion and the pressure distribution on its hull for regular waves. The code, using potential flow theory and solving the radiation and diffraction problems, gave the velocity potentials for each ship motion. The added mass, the damping coefficients and the excitation forces were calculated by integrating the velocity potentials. The next step was the calculation of the ship's response and the pressure distribution on the vessel's hull was calculated, using the "dynamic Bernoulli" formula.

The vessel's response in waves was evaluated for different ship's headings and speeds, and for different wave frequencies.

From the above hydrodynamic analysis, the SWATH -type ships were found to have good rolling characteristics. This is due to the larger moment of inertia they present around the longitudinal axis of rotation making them better than monohulls of the same displacement.

On the other hand, for certain combinations of frequency, ship's speed and heading, the amplitude of the excitation may acquire large values, especially as to heave and pitch motions (rotation over the transversal axis and vertical displacement respectively). For this reason forward and aft fins (canards and stabilizers) should be added.

Having evaluated the hull's pressure distribution for different sea states, the ship's structural response was calculated using the ADINA code. The resultant stresses and the impact of the ship's structural design were discussed in Chapter 3. The area of higher stresses was found to be where the inner side of the struts join the platform (haunch). Increasing the radius of curvature and using high strength steel (a practice recommended by the classification societies) brings the stresses to acceptable levels. It was found that there is no need to use more than 9 elements to describe the stress distribution in the haunch accurately, when the form of a 9 foot curvature is adopted for the area under consideration.

Another topic which was discussed was the impact of fatigue loading on the ship's life. To evaluate the accumulative fatigue damage ratio, stresses were evaluated for all frequencies of the wave spectrum of the North Atlantic Sea (supposedly the area of operation of the vessel) assuming unit wave amplitude, and for all headings. For each stress amplitude S_i , the number of expected cycles over the ship's life¹ was calculated, and it was assumed that each cycle causes damage proportional to $\frac{1}{N_i}$ where N_i is the number of cycles the structure withstands without collapsing under stress load S_i . The accumulation of the damage for all cycles and all stress amplitudes gives, according to Miner's rule, the accumulative fatigue damage ratio which should not be higher than 0.3 for non-essential structural elements and 0.1 for essential or difficult to inspect elements. In our case, the accumulative fatigue damage ratio was found to be 0.02 at the haunch (area of higher stress). Therefore fatigue loads do not diminish the ship's life.

Apart from the vessel's excitation due to regular waves, there is also the concern of

¹Vessel's life was assumed 20 years

excitation due to irregular ones. The evaluation of vibrational behavior of the vessel was made by comparing the natural frequencies of the ship's structure with the wave frequencies in which large amplitude waves occur. The traditional method of calculating the natural frequencies of a ship's structure is to approximate it as a beam. As a SWATH ship cannot be approximated as a beam (as its breadth and draft are not small in comparison to its length), finite element analysis is necessary to estimate the vessel's natural frequencies. The 7th mode (the six first correspond to the six rigid body modes) corresponds to lower hull lateral vibration, a vibrational mode that does not exist in monohull ships and justifies our choice for using finite element analysis for the evaluation of natural frequencies. All modes were found to have high frequencies when compared to the wave frequencies, and therefore negligible dynamic response occurs.

Apart from wave loads, propeller loads also cause vibrations to the ship structure. They are generated because the propeller works in the ship's non-uniform wake. Propeller vibrations were discussed in chapter 4. Propellers were designed so as to have an optimum efficiency at service speed (18 knots), acceptable cavitation number (less than 20%) at maximum speed (23 knots), and meet strength criteria at all speeds. They were designed using the PLL (propeller lifting line) code.

A five blade propeller was used. It gives better efficiency than a four-bladed one and a smaller amplitude of vibration due to the smoothness that the 5 blades provide (compared with a 4 bladed propeller). A better choice that would have diminished drastically propeller vibrations would have been a counter-rotating propeller. Unfortunately, counter-rotating propellers present lower efficiency than conventional ones due to their larger hub.

After designing the propeller, the forces acting on the propeller blades were evaluated. Blades were separated in chordwise strips, the force acting on each strip evaluated and finally the total force summed up. Each blade had different loading for each position angle. Summing up the forces (vertical components only) for all the angles (full propeller rotation), we were able to evaluate the periodic (but not sinusoidal) vertical force.

Finally, using the ADINA finite element code, the response of the structure due to propeller vibrations was evaluated. Areas with the higher vibration amplitudes were located.

As was shown (fig. 4.7) those high amplitudes are still low and satisfy the classification's society's requirements (ISO 9000 in this case).

Appendix A

Plates and stiffeners catalog.

a. Stiffeners

No	Stiffener size	A [in.sq.]	I [in.4]	C [in]	D [in]	TW [in]	BF	TF
1	4x4x5	1.44	2.98	2.1	3.95	0.170	3.94	0.205
2	5x4x6	1.73	3.55	4.3	4.94	0.190	3.96	0.210
3	6x4x9	1.81	4.22	6.5	5.90	0.170	3.94	0.215
6	8x4x10	2.11	5.35	14.2	7.89	0.170	3.94	0.205
24	12x4x14	3.23	7.49	49.5	11.91	0.200	3.97	0.225
28	12x4x16	3.64	7.61	56.5	11.99	0.220	3.99	0.265
33	10x4x19	4.05	6.93	45.2	10.24	0.250	4.02	0.395
35	12x4x19	4.18	7.95	66.7	12.16	0.235	4.01	0.350
40	14x5x22	4.76	9.12	97.4	13.74	0.230	5.00	0.335
45	12x6x26	5.19	8.82	80.2	12.22	0.230	6.49	0.380
49	14x5x26	5.55	9.39	115.5	13.91	0.255	5.03	0.420
51	16x5x26	5.73	10.27	153.4	15.69	0.250	5.50	0.345
58	14x6x30	6.22	9.61	127.3	13.84	0.270	6.73	0.385
60	16x5x31	6.68	10.61	181.9	15.88	0.275	5.53	0.440
81	18x7x50	10.46	12.39	360.9	17.99	0.355	7.50	0.570

b. Plates

Code Number	Thickness [in]	Weight [psf]
6	0.2813	11.048
7	0.3125	12.75
8	0.3438	14.03
9	0.3750	15.30
10	0.4375	17.85
11	0.5000	20.40
14	0.6875	28.05

Appendix B

Data for calculation of propeller loads.

$G_{in} = \frac{\Gamma_{in}}{\pi D V_s}$: the non-dimensional circulation.

R/R_0	0	30	60	90	120	150	180	210	240	270	300	330
0.20	.0167	.0168	.0170	.0169	.0168	.0169	.0170	.0170	.0166	.0167	.0172	.0169
0.25	.0170	.0171	.0173	.0171	.0171	.0171	.0173	.0172	.0168	.0169	.0174	.0171
0.30	.0195	.0197	.0199	.0197	.0196	.0197	.0199	.0198	.0194	.0195	.0200	.0197
0.40	.0253	.0255	.0257	.0256	.0255	.0256	.0258	.0257	.0251	.0252	.0260	.0255
0.50	.0300	.0302	.0305	.0303	.0301	.0303	.0305	.0304	.0297	.0299	.0307	.0302
0.60	.0331	.0333	.0337	.0334	.0333	.0334	.0337	.0336	.0328	.0330	.0339	.0333
0.70	.0345	.0348	.0351	.0349	.0347	.0348	.0351	.0350	.0342	.0344	.0354	.0348
0.80	.0335	.0338	.0341	.0339	.0337	.0339	.0342	.0341	.0333	.0335	.0344	.0338
0.90	.0281	.0283	.0286	.0284	.0282	.0283	.0286	.0285	.0279	.0280	.0288	.0283
0.95	.0217	.0219	.0221	.0220	.0219	.0219	.0221	.0221	.0216	.0217	.0223	.0219
1.00	.0000	.0000	.0000	.0000	.0000	.0000	.0000	.0000	.0000	.0000	.0000	.0000

β_i : the hydrodynamic angle of advance in degrees. This pitch angle includes the velocities induced by the propeller.

R/R_0	0	30	60	90	120	150	180	210	240	270	300	330
0.20	42.12	43.20	41.28	39.98	35.60	42.32	41.17	42.79	46.59	44.13	42.48	44.96
0.25	37.30	38.88	38.17	37.77	34.47	39.56	38.46	40.42	42.44	39.95	38.35	39.15
0.30	34.22	35.97	36.10	35.94	33.49	37.44	36.33	38.20	39.30	37.22	35.71	35.42
0.40	30.15	31.98	32.93	32.63	31.35	33.84	32.74	33.85	34.47	33.61	32.18	31.07
0.50	26.91	28.88	29.96	29.44	28.82	30.45	29.46	29.76	30.49	30.65	29.28	28.26
0.60	24.05	26.34	27.16	26.69	26.30	27.44	26.74	26.64	27.20	27.75	26.63	25.92
0.70	21.47	24.23	24.67	24.53	24.07	24.98	24.67	24.73	24.55	24.81	24.21	23.63
0.80	19.02	22.18	22.50	22.51	22.01	22.79	22.51	22.74	22.25	22.17	22.10	21.26
0.90	16.73	20.00	20.47	20.40	20.10	20.68	20.21	20.51	20.19	19.98	20.14	18.99
0.95	15.67	18.84	19.46	19.27	19.21	19.63	19.05	19.34	19.25	19.09	19.17	17.97
1.00	14.69	17.62	18.42	18.10	18.38	18.58	17.89	18.15	18.36	18.34	18.18	17.04

$\frac{U_a}{V_s}$ The axial velocity divided by the ship speed.

R/R_0	0	30	60	90	120	150	180	210	240	270	300	330
0.20	.5821	.6551	.5503	.6166	.4706	.5033	.5973	.6278	.7816	.7040	.5671	.6876
0.25	.6181	.6886	.6244	.6768	.5584	.5799	.6594	.7132	.8234	.7397	.6088	.6797
0.30	.6485	.7203	.6892	.7271	.6337	.6460	.7104	.7729	.8581	.7789	.6517	.6858
0.40	.6941	.7799	.7945	.8046	.7526	.7522	.7876	.8368	.9099	.8609	.7375	.7289
0.50	.7230	.8368	.8730	.8626	.8385	.8318	.8456	.8643	.9450	.9350	.8177	.7945
0.60	.7390	.8942	.9313	.9144	.9025	.8948	.9013	.8999	.9717	.9863	.8852	.8602
0.70	.7443	.9507	.9755	.9682	.9535	.9509	.9628	.9720	.9957	.0039	.9352	.9041
0.80	.7344	.9839	.0073	.0040	.9877	.0028	.9960	.0222	.0118	.0018	.9717	.9152
0.90	.7175	.9850	.0224	.0113	.0089	.0371	.9950	.0302	.0205	.0015	.9922	.9081
0.95	.7103	.9726	.0223	.0027	.0168	.0425	.9832	.0178	.0231	.0084	.9948	.9040
1.00	.7060	.9510	.0163	.9850	.0241	.0372	.9654	.9942	.0252	.0234	.9915	.9028

$\frac{u_a}{V_s}$: the induced axial velocity divided by the ship speed.

R/R_0	0	30	60	90	120	150	180	210	240	270	300	330
0.20	.0735	.0322	.0261	.0264	.0133	.0302	.0316	.0358	.0427	.0368	.0273	.0412
0.25	.1134	.0710	.0665	.0669	.0572	.0689	.0716	.0737	.0775	.0745	.0676	.0794
0.30	.1547	.1109	.1069	.1073	.1003	.1076	.1117	.1117	.1134	.1128	.1086	.1196
0.40	.2307	.1834	.1789	.1792	.1758	.1767	.1837	.1805	.1792	.1816	.1825	.1939
0.50	.2851	.2351	.2294	.2301	.2281	.2257	.2348	.2302	.2269	.2301	.2346	.2468
0.60	.3202	.2686	.2624	.2634	.2618	.2581	.2682	.2635	.2586	.2617	.2685	.2809
0.70	.3428	.2920	.2859	.2868	.2854	.2814	.2917	.2870	.2813	.2843	.2923	.3040
0.80	.3558	.3101	.3049	.3055	.3039	.3004	.3103	.3058	.2995	.3025	.3110	.3209
0.90	.3560	.3211	.3174	.3176	.3156	.3133	.3221	.3183	.3112	.3138	.3229	.3294
0.95	.3504	.3230	.3202	.3202	.3178	.3164	.3244	.3211	.3135	.3159	.3252	.3296
1.00	.3408	.3220	.3202	.3201	.3172	.3168	.3237	.3210	.3130	.3149	.3247	.3265

$\frac{u_t}{V_s}$: the tangential component of induced velocity divided by the ship speed.

R/R_0	0	30	60	90	120	150	180	210	240	270	300	330
0.20	-1.55	-1.54	-1.57	-1.57	-1.61	-1.54	-1.57	-1.54	-1.47	-1.52	-1.58	-1.54
0.25	-1.52	-1.51	-1.53	-1.52	-1.53	-1.50	-1.53	-1.51	-1.46	-1.49	-1.54	-1.52
0.30	-1.52	-1.52	-1.53	-1.52	-1.52	-1.51	-1.53	-1.52	-1.49	-1.50	-1.55	-1.53
0.40	-1.55	-1.56	-1.57	-1.56	-1.55	-1.56	-1.57	-1.57	-1.54	-1.54	-1.58	-1.56
0.50	-1.51	-1.52	-1.54	-1.53	-1.52	-1.53	-1.54	-1.54	-1.51	-1.51	-1.55	-1.52
0.60	-1.41	-1.49	-1.45	-1.44	-1.43	-1.44	-1.45	-1.45	-1.42	-1.43	-1.46	-1.43
0.70	-1.30	-1.34	-1.36	-1.35	-1.34	-1.35	-1.36	-1.35	-1.32	-1.33	-1.37	-1.33
0.80	-1.18	-1.25	-1.27	-1.26	-1.25	-1.27	-1.27	-1.27	-1.24	-1.24	-1.28	-1.23
0.90	-1.04	-1.14	-1.18	-1.16	-1.16	-1.17	-1.16	-1.17	-1.14	-1.15	-1.18	-1.12
0.95	-0.96	-1.08	-1.12	-1.10	-1.11	-1.12	-1.10	-1.10	-1.09	-1.10	-1.12	-1.06
1.00	-0.88	-1.00	-1.05	-1.03	-1.05	-1.05	-1.03	-1.03	-1.03	-1.04	-1.06	-0.99

Appendix C

Fatigue load calculations.

To calculate the accumulative fatigue loads, the following steps were taken:

The wave spectrum of North Sea was “discretized” in blocks which correspond to the frequencies in which the vessel was tested. For 10,000 observances of wave’s crests, the table C.1 was derived from table 3.2

The frequencies that are not shown are either very small or very large to cause significant stress or the probability to occur is very small.

Assuming linear dependence between stress and wave heights, and knowing the resultant stress for each frequency and for 1 ft. wave height (table), the following table was derived :

Let us recall Miner’s rule :

Freq. [deg/sec]	Number of occurrences at corresponding wave heights							
	3 ft.	4 ft.	5 ft.	6 ft.	7 ft.	8 ft.	9 ft.	10 ft.
528.83	462	221	8	0	0	0	0	0
431.81	1,061	1,233	146	6	0	0	0	0
373.96	1,569	3,223	831	85	4	0	0	0
334.47	817	2,553	1,147	240	28	2	0	0
305.31	817	2,553	1,147	240	28	2	0	0
282.667	908	3,876	2,597	914	210	26	1	0
264.415	782	3,699	2,867	1,259	404	82	10	1
249.29	655	3,522	3,138	1,604	600	138	18	1
236.511	643	4,102	4,456	2,960	1,564	571	136	20

Table C.1: New wave spectrum.

Freq. [deg/sec]	Sresses 3 ft.	in 4 ft.	corresponding 5 ft.	wave 6 ft.	heights 7 ft.	8 ft.	9 ft.	10 ft.
528.83	238.7	477.5	716.2	955.0	1,193.7	1,432.4	1,671.2	1,909.9
431.81	264.6	529.3	793.9	1,058.5	1,323.1	1,587.8	1,852.4	2,117.0
373.96	207.3	414.6	621.9	829.1	1,036.4	1,243.7	1,451.0	1,658.3
334.5	215.1	430.3	645.4	860.6	1,075.7	1,290.9	1,506.0	1,721.2
305.3	401.3	802.7	1,204.0	1,605.4	2,006.7	2,408.1	2,809.4	3,210.7
282.7	403.2	806.4	1,209.5	1,612.7	2,015.9	2,419.1	2,822.3	3,225.5
264.4	236.6	473.2	709.9	946.5	1,183.1	1,419.7	1,656.3	1,893.0
249.3	138.9	277.8	416.7	555.6	694.5	833.4	972.3	1,111.2
236.511	100.3	200.5	300.8	401.0	501.3	601.5	701.8	802.0

Table C.2: Resultant stress in $[\frac{lb}{ftsec^2}]$ for given frequency and wave height.

$$\sum_{i=1}^b \frac{n_i}{N_i} < n_L$$

In this case, $b = 9$, as there are 9 frequencies-stress blocks, n_i is given in table C.1, and N_i is derived from the “S-N” curves (fig. 3.16) and table C.2.

The nondimensional damage ratio n_L is evaluated by adding up all the ratios for each combination of stress-frequency. It is found to be 0.02, much lower than the $n_{L_{max}} = 0.1$ which is required by the classification societies for vital structural elements.

Appendix D

Propeller data.

PLL VERSION 4.1 SUMMARY OUTPUT

SHIP SPEED (ft/sec):	38.90	FLUID DENSITY:	1.9900
SHAFT DEPTH (ft):	13.20	PROP. COMPONENTS:	1
TOTAL THRUST (lbs):	276243.41	HORSEPOWER:	26125.654
EFFICIENCY:	0.679	VOL.MN.VEL.(1-W):	0.908
IMAGE HUB USED:	T	HUB DRAG (lbs):	3486.15
TIP GAP FACTOR:	1.0000	EXPANDED AREA RATIO:	0.530
HUB DRAG (lbs):	3486.15	(HUB VORTEX)/(RHUB):	0.5000
AXIAL LOCATION(ft):	0.00	DIAMETER (ft):	15.00
NUMBER OF BLADES:	5	HUB DIAMETER (ft):	3.00
NUMBER OF PANELS:	10	REVS. PER MINUTE:	200.00
WAKE DIAMETER (ft):	15.00		
TORQUE (ft-lbs):	686074.50	HORSEPOWER:	26125.654
J SHIP:	0.778	VOLUMETRIC J:	0.706
BLADE VOLUME (ft**3):	26.4443	MOM INERTIA (ft**5):	391.87
THRUST (lbs):	279729.56		

Table D.1: Propeller data.



Institute Archives and Special Collections
Room 14N-118
The Libraries
Massachusetts Institute of Technology
Cambridge, Massachusetts 02139-4307

This is the most complete text of the thesis available. The following page(s) were not included in the copy of the thesis deposited in the Institute Archives by the author: 79

Bibliography

- [1] Gilmer, T. C. and Johnson, B., *“Introduction to Naval Architecture,”* Naval Institute Press, Annapolis, Maryland, 1982.
- [2] Faltinsen, O. M., *“Sea loads on ships and offshore structures,”* Cambridge University Press, Cambridge, Massachussets, 1990.
- [3] Newman, J. N., *“Marine Hydrodynamics,”* M.I.T. Press, Cambridge, Massachussets, 1977.
- [4] Hughes, O. F., *“SHIP STRUCTURAL DESIGN. A rationally-based, computer-aided optimization approach,”* SNAME, Jersey City, New Jersey, 1988.
- [5] *“ADINA user’s manual,”* ADINA R&D, Inc., Watertown, Mass., December 1992.
- [6] Bourceau, G. and Volcy, G. C., *“Forced vibration resonators and free vibration hull,”* Machinery hull interaction - Vibrations, pp. 109-150, Bureau Veritas, Paris, 1977.
- [7] Clark, M. R., Nguyen L. B. et al., *“Structural design, stress analysis and hull structure weight estimates for a 4000 ton SWATH TAGX,”* DWTNS-RDC, Bethesda, Maryland, November 1985.
- [8] Covich, P., *“T-AGOS 19: An innovative program for an innovative design,”* Naval Engineers Journal, pp. 99-106, May 1987.
- [9] Reilly, E. T., Shin Y. S. et al., *“A prediction of structural load and response of a swath ship in waves,”* Naval Engineers Journal, pp. 251-264, May 1988.

- [10] Gupta, S. K. and Schmidt, T. W., "*Developments of a SWATH design*," Naval Engineers Journal, pp. 171-188, May 1986.
- [11] Gore, J. L., "*SWATH ships*," Naval Engineers Journal, pp. 83-112, February 1985.
- [12] Cazaud, R., "*Fatigue of metals*," Philosophical Library, New York, 1953.
- [13] Pegg, N. G. and Gilroy, L.E., "*Full scale verification of finite element modelling of a 75 tonne SWATH vessel*," Marine Structures, Elsevier Science Limited, Great Britain, 27 January 1994.
- [14] Salvesen, N. , v.Kerczek, C. H. et al., "*Hydro-numeric design of SWATH ships*," SNAME, Transactions, pp. 325-346, Vol. 93, 1985.
- [15] SNAME, Panel HS-7, "*Guide for the analysis and evaluation of shipboard hull vibration data*," SNAME, Thecnical and Research Bulletin 2-29, 1984.
- [16] Newman, J. N., "*The evaluation of free surface Green functions*," 4th Int. Conference on numerical ship hydrodynamics, pp.4-20, Washington, 1985.
- [17] Newman, J. N., "*Algorithms for the free surface Green function*," Journal of Engineering Mathematics, pp. 57-67, Vol. 19,1985.
- [18] McCreight, K. M., "*Assessing the seaworthiness of SWATH ships*," SNAME, Transactions, pp. 189-214, Vol.95, 1987.
- [19] Bathe, K.J., "*Finite element procedures in engineering analysis*," Prentice-Hall, Inc., Englewood Cliffs, New Jersey 07632, 1982.